VHL deficiency drives enhancer activation of oncogenes in clear cell renal cell carcinoma

Xiaosai Yao[1,2]*, Jing Tan[3]*, Kevin Junliang Lim*[4], Joanna Koh[1], Wen Fong Ooi[1], Zhimei Li[3], Dachuan Huang[3], Manjie Xing[1, 4, 5], Yang Sun Chan[1], James Zhengzhong Qu[1], Su Ting Tay[4], Giovani Wijaya[3], Yue Ning Lam[1], Jing Han Hong[4], Ai Ping Lee-Lim[1], Peiyong Guan[3], Michelle Shu Wen Ng[2], Cassandra Zhengxuan He[1], Joyce Suling Lin[1], Tannistha Nandi[1], Aditi Qamra[1,6], Chang Xu[4,7], Swe Swe Myint[3], James O. J. Davis[8], Jian Yuan Goh[1], Gary Loh[1], Bryan C. Tan[9], Steven G. Rozen[4], Qiang Yu[1], Iain Bee Huat Tan[1,10], Christopher Wai Sam Cheng[11], Shang Li[4], Kenneth Tou En Chang[12], Puay Hoon Tan[13], David Lawrence Silver[9], Alexander Lezhava[14], Gertrud Steger[15], Jim R. Hughes[8], Bin Tean Teh[2,3,4,7,16]**, Patrick Tan[1,4,6,7,16]**&

Affiliations

[1]Cancer Therapeutics and Stratified Oncology, Genome Institute of Singapore, 60 Biopolis Street, Genome #02-01, Singapore 138672, Singapore

[2]Institute of Molecular and Cell Biology, 61 Biopolis Drive, Singapore 138673, Singapore

[3]Laboratory of Cancer Epigenome, Department of Medical Sciences, National Cancer Centre, 11 Hospital Drive, Singapore 169610, Singapore

[4]Cancer and Stem Cell Biology Program, Duke-NUS Graduate Medical School, 8 College Road, Singapore 169857, Singapore

[5]NUS Graduate School for Integrative Sciences and Engineering, National University of Singapore, 5 Lower Kent Ridge Road, Singapore 119074, Singapore

[6]Department of Physiology, Yong Loo Lin School of Medicine, National University of Singapore, 2 Medical Drive #04-01, Singapore 117597, Singapore

[7]Cancer Science Institute of Singapore, National University of Singapore, 14 Medical Drive, #12-01, Singapore 117599, Singapore

[8]Medical Research Council (MRC) Molecular Haematology Unit, Weatherall Institute of Molecular Medicine, Oxford University, Oxford OX3 9DS, United Kingdom

[9]Cardiovascular & Metabolic Disorders Programme, Duke-NUS Graduate Medical School, 8 College Road, Singapore 169857, Singapore

[10]Division of Medical Oncology, National Cancer Centre Singapore, 11 Hospital Drive, Singapore 169610, Singapore

[11]Department of Urology, Singapore General Hospital, Outram Road, Singapore 169608, Singapore.

[12]Department of Pathology and Laboratory Medicine, KK Women's and Children's Hospital, 100 Bukit Timah Road, Singapore 229899, Singapore

[13]Department of Pathology, Singapore General Hospital, 20 College Rd, Singapore 169856, Singapore

[14]Translational Research, Genome Institute of Singapore, 60 Biopolis Street, Genome #02-01, Singapore 138672, Singapore

[15]Institute of Virology, University of Cologne, Albertus-Magnus-Platz, 50923 Köln, Germany

[16]SingHealth/Duke-NUS Institute of Precision Medicine, National Heart Centre Singapore, 168752, Singapore

***These authors contributed equally to the work**

****Corresponding authors**

Running title: *VHL*-driven enhancer malfunction in ccRCC

Keywords: ccRCC; epigenetics; enhancers; VHL; HIF; ZNF395

Financial support: This work was supported by core funding from the Genome Institute of Singapore and Institute of Molecular and Cell Biology under the Agency for Science, Technology and Research, Biomedical Research Council Young Investigator Grant 1510851024, National Medical Research Council grants NMRC/STaR/0026/2015, NMRC/CIRG/1402/2014 and CBRG/069/2014, and National Research Foundation grant NRF2016NRF-NSFC001-057. Other sources of support include the Cancer Science Institute of Singapore, NUS, funded by the National Research Foundation Singapore and the Singapore Ministry of Education under its Research Centres of Excellence initiative. J.R.H. was supported by a Wellcome Trust Strategic Award (reference 106130/Z/14/Z) and Medical Research Council (MRC) Core funding. J.O.J.D. was funded by Wellcome Trust Clinical Research Training Fellowship (ref 098931/Z/12/Z).

Corresponding information:
Patrick Tan
Address: Duke-NUS Graduate Medical School, 8 College Road, Singapore 169857, Singapore
Phone: +65 6516 1783
Fax: +65 6221 2402
Email: gmstanp@duke-nus.edu.sg

Bin Tean Teh
Address: Duke-NUS Graduate Medical School, 8 College Road, Singapore 169857, Singapore
Phone: +65 6601 1324
Fax: +65 6221 2402
teh.bin.tean@singhealth.com.sg

The authors declare no conflict of interests

Total word count: 7261
Total figure count: 7

Abstract

Protein coding mutations in clear cell renal cell carcinoma (ccRCC) have been extensively characterized, frequently involving inactivation of the von Hippel Lindau (*VHL*) tumor suppressor. However, how non-coding cis-regulatory aberrations drive ccRCC tumorigenesis remains to be clarified. Analyzing 79 chromatin profiles of primary ccRCCs, matched normal kidney tissues and cell lines, we observed pervasive enhancer malfunction in ccRCC, with cognate enhancer-target genes associated with tissue-specific aspects of malignancy. Super-enhancer profiling identified *ZNF395* as a ccRCC-specific and *VHL*-regulated master regulator, whose depletion causes near-complete tumor elimination *in vitro* and *in vivo*. We show that *VHL* loss predominantly drives enhancer/super-enhancer deregulation more so than promoters, with acquisition of active enhancer marks (H3K27ac and H3K4me1) near ccRCC hallmark genes. Mechanistically, *VHL* loss stabilizes HIF2α-HIF1β heterodimer binding at enhancers, leading to recruitment of histone acetyltransferase P300 but without overtly affecting pre-existing promoter-enhancer interactions. Subtype-specific driver mutations such as *VHL* may thus propagate unique pathogenic dependencies in ccRCC through the modulation of *cis*-regulatory epigenomic landscapes and cancer gene expression.

Significance

Comprehensive epigenomic profiling of ccRCC establishes a compendium of somatically altered *cis*-regulatory elements, uncovering new potential targets including *ZNF395*, a ccRCC master regulator. Loss of *VHL*, a ccRCC signature event, causes pervasive enhancer malfunction, with binding of enhancer-centric HIF2α and recruitment of histone acetyltransferase P300 at pre-existing lineage-specific promoter-enhancer complexes.

Introduction

Clear cell renal cell carcinoma (ccRCC) is the most common subtype of kidney cancer with 338,000 new cases in 2012 worldwide [1]. With most ccRCCs being radio-chemo-resistant, metastatic ccRCC patients exhibit dismal 8% five-year overall survival [2]. While targeted therapies inhibiting angiogenesis and mTOR pathways can lead to initial tumor control, most patients develop resistance in less than a year [3, 4]. A better understanding of ccRCC molecular dependencies and vulnerabilities is thus needed to develop new therapeutic strategies for patients who fail standard of care treatment.

Loss of the von Hippel-Lindau (*VHL*) tumor suppressor is a defining feature of ccRCC [5, 6]. When partnered with additional tumor suppressors (*PBRM1*, *BAP1, TP53* and/or *RB1*), *VHL* loss drives spontaneous ccRCC formation in mouse models ([7-9]). *VHL* encodes an E3 ubiquitin ligase [10, 11] that targets hypoxia-inducible factor (HIF)-1α (*HIF1A*) and HIF2α (*EPAS1*), for degradation [12, 13]. *VHL* loss in ccRCC results in constitutive activation of HIF1/2α, and subsequent transactivation [14, 15] of downstream genes regulating angiogenesis, glycolysis [16], lipogenesis [17, 18], cell cycle [19] and anti-apoptosis [20].

Most reports studying VHL/HIF transcriptional activation have focused on HIF-bound promoters [21-26]. However, recent evidence suggests an emerging role for distal enhancer elements in VHL/HIF transcriptional control [27, 28]. For example, HIF2α-bound distal enhancers activate the proto-oncogenes *MYC* [29] and *CCND1* [19], and coincide with ccRCC genetic risk alleles. Nevertheless, such studies focused on individual enhancers, and the majority of distal elements in ccRCC remain largely unexplored.

Delineating the global ccRCC *cis*-regulatory landscape may also identify novel master regulators involved in tissue-specific disease processes. Compared to promoters that are largely cell-type invariant, distal enhancers integrate multiple lineage- and context-dependent

signals, catering to the specialized needs of diverse cell types and diseases [30, 31]. In cancer, such master regulators are frequently located near “super-enhancers” or “stretch-enhancers” marked by long stretches of H3K27ac signals [32, 33]. For example, subtype-specific genomic alterations such as *EGFRvIII* in glioblastoma [34] and *EWS-FLI* in Ewing’s sarcoma [35] induce *de novo* enhancers, causing reactivation of developmental master regulators required for self-renewal and lineage specification [34]. While *VHL* inactivation has been shown to modulate protein levels of different histone modifiers (e.g. KDM5C/JARID1C [36], HDAC1 [37], JMJD1A [38], JMJD2B [38] and JMJD2C [39]), the impact of these protein alterations at specific epigenomic loci remains unclear. Moreover, previous studies profiling histone modifications in ccRCCs have also been limited by small sample sizes (2 cases, [40]), reliance on *in vitro* systems, and the lack of long-range interactome data and functional enhancer testing to accurately assign cognate enhancer targets.

In this study, we establish the most comprehensive collection of ccRCC histone profiles to date, annotating the precise genomic locations of altered promoters, enhancers and super-enhancers in ccRCC. Using isogenic cell lines with or without wild-type *VHL,* we further demonstrate that besides its well-defined role in oxygen sensing, *VHL* also safeguards the chromatin landscape; its loss induces tumor-specific enhancer gains around ccRCC hallmark genes such as angiogenic and metabolic targets through the stabilization of HIF2α/HIF1β (*ARNT*) heterodimers and recruitment of P300 histone acetyltransferase (*EP300*). One important target of epigenetic activation is *ZNF395*, a master regulator of ccRCC tumorigenesis. Taken collectively, our results reveal an epigenetic framework by which the major ccRCC-specific driver mutation, *VHL*, induces *de novo* enhancers, contributing to oncogenic transcription.

Results

Cis-regulatory landscapes in ccRCC tumors are aberrant

To explore whether ccRCCs display alterations in their *cis*-regulatory landscapes *in vivo*, we generated histone ChIP-seq profiles (3 marks: H3K27ac, H3K4me3, H3K4me1) in 10 normal-primary tumor ccRCC pairs, 5 patient-matched tumor-derived cell lines, 2 commercially available ccRCC lines (786-O, A-498) and 2 normal kidney cell lines (HK-2, PCS-400) (Refer to **Table S1** for patient clinical information). Of the original 87 samples, 79 samples passed pre-sequencing quality control filters and were subjected to ChIP-seq processing and downstream analysis. In total, we generated 2,363,904,778 uniquely mapped reads (Refer to **Table S2** for sequencing statistics). On average, 89% of H3K27ac peaks, 98% of H3K4me3 peaks and 76% of H3K4me1 peaks obtained in our normal kidney tissues overlapped with peaks from adult kidney tissues in the Epigenomics Roadmap dataset **(Figure S1A).** Among the 10 primary ccRCCs, 9 harbored *VHL* mutations, detected by targeted sequencing and confirmed by Sanger sequencing (**Table S3**). Cell lines 786-O and A-498 also harbor *VHL* truncating mutations (**Table S3**). The *VHL* mutations co-occurred with somatic mutations of other chromatin modifiers commonly found in ccRCC, including *PBRM1* (7/10), *SETD2* (1/10), *KDM5A* (1/10), *KDM5C* (1/10)*, ARID1A* (1/10) *and KMT2C* (1/10).

Specific histone modifications can distinguish different categories of functional regulatory elements - H3K4me3 is generally associated with promoters, H3K4me1 with enhancers and H3K27ac with active elements [31, 41]. Integrating signals from 3 histone marks and GENCODE v19 annotated transcription start sites (TSS), we defined active promoters as H3K27ac^{+}/H3K4me3^{+}/±2.0 kb TSS regions, and distal enhancers as H3K27ac^{+}/H3K4me1^{+} regions not overlapping with promoters. Focusing on epigenomic events specific to somatic cancer cells, we derived cell lines from 5 primary tumors and, combined with the commercial

lines, excluded peaks not found in any of the cell lines to reduce confounding effects from stromal cells. On average, we observed 80% overlap of ChIP-seq peaks between primary tumors and matched lines **(Figure S1B**). Using these criteria, we identified 17,497 putative promoters and 66,448 putative enhancers **(Figure 1A)**, numbers comparable to previous studies in other tumor types [41-43]. The numbers of defined promoters and enhancers reached saturation after 4 and 16 samples respectively, indicating that a sample size of 20 (10 normal/tumor pairs) is likely sufficiently powered to discover the majority of *cis*-regulatory elements in ccRCC (**Figure S1C, D**). Principal components analysis (PCA) using the first 2 components of global H3K27ac intensities at promoters or enhancers (representing 83% and 64% of total variance respectively **Figure S1E, F**) successfully separated normal and tumor samples, indicating that genome-wide pervasive alterations in *cis*-regulatory elements are a salient feature of ccRCC **(Figure 1B)**.

We performed differential analysis to identify altered promoters and enhancers. To define gained or lost regions, we applied a fold difference of H3K27ac RPKM ≥ 2, an absolute difference ≥ 0.5, and for greater stringency no alterations in the reverse direction in the remaining tumor/normal pairs (see Methods and **Figure S1G** for distribution of altered elements by number of patients). At the threshold of ≥5/10 patients, 80% of the altered regions achieved statistical significance (q-value < 0.1, paired t-test, with Benjamini-Hochberg correction) (**Figure S1H**) and at this same threshold, the increase in the fraction of samples meeting statistical significance reached a saddle point (**Figure S1I**). Applying these criteria, we obtained a high-confidence and comprehensive set of 4,719 gained promoters, 592 lost promoters, 4,906 gained enhancers, and 5,654 lost enhancers (**Figure 1A, C, Table S4**). Representative regions are presented in **Figure S2**.

Supporting the reliability of this data, gained promoters and enhancers exhibited increased chromatin accessibility measured by higher FAIRE-Seq signals [44] in tumor tissues than

normal tissues respectively (*p*-value < 0.0001), and also decreased DNA methylation based on TCGA data [45], consistent with reciprocal relationships between active regulatory regions and DNA methylation (**Figure 1D)**. Interestingly, we also noted elevated expression of long non-coding RNAs [46] adjacent to gained promoters and enhancers in tumor tissues compared to normal tissues (*p*-value < 0.0001 respectively). Lastly, we confirmed that many of our *cis*-regulatory elements involved regions previously implicated in ccRCC – for example, we observed gains of H3K27ac signals and enrichment of H3K4me1 at a distal enhancer of *CCND1* overlapping with an RCC susceptibility locus (rs7105934 [47] [19]) **(Figure 1E).** Our ability to re-discover this important enhancer in our unbiased profiling supports our data reliability.

Tumor-specific enhancers are associated with hallmarks of ccRCC

To identify genes modulated by the tumor-specific regulatory elements, we assigned enhancers using three approaches. The first approach utilized pre-defined linear proximity rules involving a set of highly confident genes (GREAT algorithm) [48] (**Table S5**). MSigDB pathway analysis using GREAT-assigned genes revealed that gained enhancers exhibit a highly significant RCC-specific signature compared to gained promoters (enhancer *q*-value = 3.2x 10^{-26}; promoter *q*-value = 1.5 x 10^{-1}, binomial FDR) (**Figure 2A).** While gained promoters were involved in general cancer processes (e.g. cell cycle, transcription and RNA metabolism, see **Table S6** for a complete list of promoter pathways), gained enhancers were enriched in disease-specific features of ccRCC including HIF1α network activity, pro-angiogenic pathways (platelet activation, PDGFRβ signaling), and SLC-mediated transmembrane transport (**Figure 2A, Table S7** for a complete list of enhancer pathways**)**. Notably, HIF1α network activity consistently emerged as one of the top 5 pathways, even with perturbations in the patient thresholds used to defined gained enhancers (≥ 3-8 patients) (**Table S8).**

Individual genes associated with gained enhancers included well-known hypoxic targets (*VEGFA* (**Figure 2B**), *CXCR4*) and metabolic genes involved in glycolysis, glutamine intake and lipid storage (*GLUT1/SLC2A1* (**Figure 2C**), *HK2, PFKFB3, PLIN2* (**Figure S3A)** and *SLC38A1* (**Figure S3B)** [49]). The presence of enhancers around metabolic enzymes and transporters is largely consistent with the metabolic contexture of ccRCC, which involves increased glycolysis and glutaminolysis [17, 50-53]. Indeed, gene ontology (GO) analysis of gained enhancers strongly reflected hallmark metabolic changes associated with ccRCC, including monocarboxylic acid transmembrane transporter activity (binomial FDR *q*-value = 1.6 $x10^{-10}$) (**Figure S3C**).

We also used a second method of enhancer-gene assignment based on correlations between H3K27ac signals and expression of genes within the same topological associated domain (TAD) [32]. Using a *q*-value <0.05 based on Spearman's correlation, we assigned 2311 gained enhancers to 2186 protein-coding targets (**Table S9**). Reassuringly, H3K27ac signals of many gained enhancers were highly correlated with gene expression of their putative target genes. For example, H3K27ac levels of a *VEGFA* enhancer exhibited high correlation with *VEGFA* gene expression (r = 0.83, Spearman's correlation), while H3K27ac signals of a *SLC2A1* enhancer were highly correlated with *SLC2A1* gene expression (r = 0.72, Spearman's correlation) (**Figure 2B**, **Figure S3D**). Similar to the GREAT approach, the TAD correlation approach also highlighted hypoxia (Krieg_Hypoxia_not_via_KDM3A, FDR *q*-value = 7 x 10^{-120}) and metabolism (Chen_Metabolic_Syndrome_Network, FDR *q*-value = 2 x 10^{-91}) as highly enriched pathways (**Table S10**).

Thirdly, to independently validate the GREAT and TAD approaches in the specific context of ccRCC, we experimentally explored the interactome of ccRCC tumor-specific enhancers by performing Capture-C assays [54]. Compared to other chromatin capture techniques, Capture-C offers both high-resolution (down to single Kb resolution) and high-throughput interrogation of

user-defined regions (a usual working range of 10-500 regions). We designed probes against a subset of 56 gained enhancers and examined their interactions with protein-coding genes in 786-O cells. Each gene-enhancer pair revealed by Capture C was further filtered by correlations between gene expression and H3K27ac levels (*q*-value <0.05). The 56 gained enhancers were paired with 36 protein-coding genes (**Table S11**) – of these, 58% were predicted by GREAT, and 80% by gene correlations within TADs. The median distance of interactions detected by Capture-C was 16 kb, and 83% of the interactions fell within a 100 kb window (**Figure S3E**). As a visual example, Capture-C confirmed interactions between *VEGFA* enhancer with the *VEGFA* TSS, spanning a distance of ~100 kb (**Figure 2B)**, and the interactions between the *SLC2A1* enhancer and its promoter (**Figure 2C)**. Taken collectively, these findings highlight the disease-specific nature of enhancer elements [31] and an important role for enhancer malfunction in modulating ccRCC pathology.

Tumor super-enhancers identify *ZNF395* as a master regulator of ccRCC tumorigenesis

The importance of enhancers in ccRCC led us to examine the landscape of "super-enhancers" or "stretch-enhancers" – dense clusters of enhancers located near master regulators of cell identity and disease [33, 55] 15. Using ROSE [33], we identified 1,451 super-enhancers in the ccRCC cohort, of which 1,157 were gained in tumor and 294 were lost in tumors (**Table S12**).

Putative targets of top gained super-enhancers validated well-known oncogenes including *MYC/PVT1*, *VEGFA and HIF2A* (**Figure 3A, Figure S4A, B).** In addition, we found several less known genes including *ERGIC1*, *ZNF395*, *SLC28A1* and *SMPDL3A* (**Figure 3B)**. These genes were highly overexpressed in tumors compared to their matched normal tissues (**Figure 3B)**. Furthermore, they were unique to ccRCC and were not overexpressed in papillary and chromophobe RCCs, two other distinct ccRCC subtypes (**Figure 3B**). For instance, *ZNF395*

exhibited a tumor-normal ratio of ~7 in ccRCC (p-value = $1x10^{-22}$, paired t-test) but experienced little over-expression in papillary and chromophobe RCC with tumor-normal ratios of 1.2 and 1.3 respectively (p-value = 0.02 in papillary and p-value = 0.06 in chromophobe, paired t-test).

Conversely, genes associated with lost super-enhancers were recurrently suppressed in ccRCC and included *EFHD1, EHF, MAL, GCOM1* and *HOXB9* (**Figure 3B)**. In contrast to the lineage-specific nature of tumor super-enhancers, genes associated with lost super-enhancers were common between ccRCC and papillary RCC, implying a more universal function of tumor suppressor genes. For example, *EHF/ESE-2*, a tumor suppressor previously found in prostate cancer [56, 57], exhibited reduced expression across all three RCC subtypes (ccRCC chromophobe tumor/normal = 0.05, p-value = 3×10^{-15}; papillary tumor/normal = 0.1, p-value $2x10^{-6}$; chromophobe tumor/normal = 0.1, p-value = $2x10^{-6}$).

Since current therapeutic targets in kidney cancer are limited to angiogenesis and mTOR pathways [3], we sought to examine these less understood genes uncovered by super-enhancer profiling. We chose *ZNF395* and *SMPDL3A* for their differential tumor expression (6-7 tumor-normal ratio) (**Figure 3B)** and high abundance (average RPKM of *ZNF395* ~112, average RPKM 58 of *SMPDL3A* ~58). Even though *ZNF395* was previously identified as a potential ccRCC biomarker [58], its functional role in ccRCC malignancy remains unexplored. *SMPDL3A* shares 31% amino acid identity with the acid sphingomyelinase *SMPD1*, and is a target of master regulator of cholesterol metabolism, Liver X Receptors (LXR) [59].

Quantitative PCR (**Figure 3C)** and immunoblotting (**Figure S4C**) confirmed that A-498 and 786-O ccRCC cells exhibited high expression of *ZNF395* and *SMPDL3A* whereas normal kidney proximal tubule cells, PCS-400 and HK-2, exhibited low expression of both genes**.** siRNA mediated knockdown of *SMPDL3A* had a cell line dependent effect on colony formation, inhibiting the growth of A-498 cells but having no observable effect on 786-O cells (**Figure 3D**).

On the other hand, *ZNF395* consistently inhibited colony formation in both 786-O and A-498 cells but had minimal effect on normal kidney cells (**Figure 3D**, **Figure S4D**). Consistent with this phenotypic observation, the *ZNF395* super-enhancer was only active in ccRCC cells (786-O, A-498) but silent in normal kidney cells (HK-2, PCS400; **Figure 3E**). Furthermore, amongst 12 types of cancers profiled by TCGA, *ZNF395* was exclusively overexpressed in ccRCC tumors, consistent with the proposed lineage- and disease-specific nature of super-enhancers (**Figure 3F**).

No study to date has functionally tested the tumorigenic requirement of *ZNF395* in ccRCC or any other cancer type. We validated *ZNF395*'s tumor-promoting effect using individual shRNA clones (**Figure S4E, F**). Two independent *ZNF395* shRNA clones drastically decreased *in vitro* colony formation (**Figure 3G**) and cell viability (**Figure 3H**) in both A-498 and 786-O cells. *ZNF395* knockdown also resulted in increased apoptosis measured by cleavage of Caspase3/7 substrates (**Figure 3I**) and Annexin V staining (**Figure S4G**). *In vivo*, tumor formation studies in mouse xenograft models revealed marked tumor suppression by *ZNF395* depletion (**Figure 3J**). Knockdown of *ZNF395* led to elimination of A-498 tumors up to day 74, when tumors in the control group began to exceed the size limits imposed by institutional animal protocols. Similarly, *ZNF395* depletion significantly slowed *in vivo* tumor growth of 786-O cells (**Figure 3J**). Taken together, we showed the indispensable role *ZNF395* plays in ccRCC tumorigenesis.

VHL **deficiency remodels ccRCC enhancer landscapes**

To explore the extent to which epigenetic changes observed in primary ccRCCs (**Figure 1**) are directly driven by *VHL* loss, we examined chromatin changes in isogenic cell lines with and without *VHL* restoration. Consistent with earlier functional studies of *VHL* [60-62], *VHL* restoration in 786-O, A-498 and 12364284 cells had negligible effects on proliferation, colony

formation and apoptosis *in vitro*, but profoundly delayed tumor growth *in vivo* (**Figure S5A-D**), suggesting the importance of *VHL* in modulating processes required for *in vivo* tumorigenesis, including tumor-stroma crosstalk, angiogenesis, cell-matrix interactions, or tumor metabolism.

Focusing on the same regions defined in the primary tumors (4,719 gained promoters, 4,906 gained enhancers and 1,157 gained super-enhancers; **Figure 1A**), we examined *VHL*-driven H3K27ac changes in 4 different cell lines (two commercial cell lines – 786-O and A-498 and two patient-derived cell lines – 12364284 and 40911432). Consistently across all 4 cell lines, *VHL* restoration induced more pronounced changes on enhancers and super-enhancers than on promoters (**Figure 4A**, **Figure S6A-C**). For example, in 786-O cells, after *VHL* restoration 12% of enhancers (549 enhancers) were significantly depleted, compared to 6.5% of promoters (321 promoters) (**Figure 4A**). We confirmed that a greater fraction of enhancers were significantly altered by *VHL* restoration than promoters ($p < 2.2 \times 10^{-16}$, proportions test), and an even higher proportion involved gained super-enhancers ($p < 2.2 \times 10^{-16}$, proportions test).

Even though gained enhancers were expected to show only depletion after *VHL* restoration, changes in H3K27ac levels were bi-directional (**Figure 4A**). However, only gained enhancers with H3K27ac depletion were uniquely active in *VHL*-mutated ccRCC cell lines (786-O, A-498, 12364284) compared to *VHL*-wild-type ccRCC cells (86049102L), normal kidney cell lines (PCS-400, HK-2 and HKC-8), and 31 other cell lines of various cancer types (**Figure 4B**). The lack of H3K27ac signals in normal kidney cell lines argues against tissue lineage as the dominant contributor to the high H3K27ac ChIP-seq signals seen in ccRCC cell lines. On the other hand, gained enhancers with H3K27ac enrichment after *VHL* restoration showed high activity across multiple cancer types, suggesting that these enhancers are not unique to ccRCC (**Figure 4B**).

Furthermore, only gained enhancers showing H3K27ac depletion after *VHL* restoration were significantly associated with a concomitant downregulation of gene expression of their putative targets in both 786-O and 12364284 cells, whereas enhancers gained in primary ccRCCs and further H3K27ac-enriched after *VHL* restoration did not lead to significant gene upregulation on a global level (**Figure 4C, S6D**). These results suggest that the former enhancers (H3K27ac depletion) are likely to represent ccRCC- and *VHL*-specific epigenomic alterations, while the latter enhancers (H3K27ac enrichment) are likely to represent signify generic, compensatory mechanisms in response to *VHL* restoration.

Combining data from multiple lines, a total of 1564 enhancers were depleted by *VHL* restoration in ≥1 cell line, representing almost a third (32%) of all gained enhancers identified in primary ccRCC tumors (**Table S13**). The proportion of *VHL*-responsive enhancers increased with the level of patient recurrence – only 7.8% of non-recurrent gained enhancers (1/10 patients) showed *VHL*-mediated H3K27ac depletion while 18% of enhancers recurrently gained in 9/10 patients and 20% of enhancers gained in 10/10 patients showed H3K27ac depletion in 786-O cells (**Figure S7A,** p-value = 0.0001, proportions test), consistent with the high prevalence of *VHL* mutations (9/10 patients) in our discovery set. Interestingly, unsupervised clustering using the 1564 *VHL*-responsive gained enhancers segregated the single *VHL* wild-type tumor (ID 75416923) away from the remaining *VHL* mutant 9 tumors (**Figure S7B**), with the *VHL*-wild-type tumor showing low H3K27ac signals at the *ZNF395* super-enhancer comparable to its patient-matched normal (**Figure S7C**). Collectively, pathway analysis of enhancers depleted in ≥2 cell lines highlighted direct p53 effectors, integrin-linked kinase signaling and HIF1α transcription factor networks as the top 5 pathways (**Table S14**), covering genes such as *EGFR* (**Figure 4D**), *CCND1* (**Figure 4E**), *ITGB3* (**Figure 4F**), *VEGFA* (**Figure 4G**), *SLC2A1* (**Figure S7D**), and *HK2* (**Figure S7E**). These results support a major role for *VHL* loss in ccRCC enhancer malfunction, even in the presence of other driver mutations.

We also examined whether other histone marks were concomitantly altered with H3K27ac marks. We found a surprisingly high degree of correlation between H3K27ac and H3K4me1 in response to *VHL* restoration in both 786-O cells (r = 0.77, Pearson's correlation, **Figure S7F**) and 12364284 (r = 0.61, Pearson's correlation, **Figure S7G**). Globally, enhancers exhibiting H3K27ac depletion also experienced concomitant H3K4me1 depletion (**Figure 4H**). We next examined whether *VHL*-restoration led to acquisition of the H3K27me3 repressive mark. Despite a moderate anti-correlation of H3K27ac and H3K27me3 (786-O cells: r = -0.28, Pearson's correlation, **Figure S7H**; 12364284 cells: r = -0.22, Pearson's correlation, **Figure S7I**), H3K27me3 levels remained low at gained enhancers even after *VHL* restoration (**Figure 4H**). These findings suggest that *VHL* restoration may result in a loss of enhancer identity by co-depletion of H3K27ac and H3K4me1, but not a formal transition to a poised enhancer state which would have retained H3K4me1 but acquired H3K27me3.

HIF2α-HIF1β heterodimer is enriched at *VHL*-responsive enhancers

We sought to investigate which transcription factors might mediate *VHL*-dependent chromatin remodeling at gained enhancers. Beginning with the primary ccRCC dataset, we looked for enrichment of *trans*-regulators in gained enhancers over lost enhancers. Using HOMER [63], we found that the top enriched motifs were AP-1 family, ETS family, NFκB-p65-Rel and HIF1α/2α motifs **(Figure 5A,** full list of motifs in **Table S15)**. For subsequent *in vitro* validation, we chose c-Jun as a representative AP-1 family member because of its activation in ccRCC [64] and ETS1 as an ETS family representative because of its known interaction with HIF2α [65], but acknowledge that other family AP-1 and ETS family members may play a role in ccRCC. Immunoblotting of c-Jun, ETS1 and NFκB-p65 showed variable protein expression in both normal and tumor cell lines, but expression of HIF1α and HIF2α restricted to tumor cells only

(Figure 5B). HIF2α was expressed in a higher proportion of ccRCC cell lines than HIF1α **(Figure 5B).** We further examined gene expression of these transcription factors in the TCGA cohort, and found that *ETS1*, *RELA* (subunit of NFκB-p65) and *HIF2α* were significantly overexpressed in tumors compared to normal tissues, with a range of tumor-association expression patterns similar to variations in ccRCC lines (**Figure S8A**).

To further investigate chromatin occupancy of these factors, we generated ChIP-seq binding profiles of c-Jun, ETS1, NFκB cells and re-examined HIF2α, HIF1α and HIF1β binding profiles from previous literature [19, 28], all performed in 786-O cells. Of note, because 786-O cells have lost endogenous *HIF1α* expression through genomic deletion, the HIF1α ChIP-seq was performed on 786-O cells genetically manipulated to re-express HIF1α protein [28]. ChIP-seq results showed that all 6 transcription factors exhibited increased occupancy at gained enhancers compared to lost enhancers, validating the HOMER predictions (**Figure 5C**).

To determine which of these transcription factors might be directly dependent on *VHL*, we then compared their protein expression in *VHL*-mutated isogenic cell lines with and without wild-type *VHL* restoration. As shown in **Figure 5D**, *VHL* restoration consistently downregulated HIF2α expression in both 786-O and 12364284 cells lines but protein levels of other factors displayed contrasting trends between the two cell lines, implying that amongst the 6 factors examined, HIF2α protein expression was the most *VHL*-dependent. Indeed, supporting an important role for HIF2α in *VHL*-dependent enhancer remodeling, only HIF2α and HIF1β were significantly enriched at enhancers showing *VHL*-dependent H3K27ac depletion (**Figure 5E**). Moreover, amongst all known motifs in the HOMER database, HIF2α was the most enriched motif at *VHL*-responsive enhancers exhibiting H3K27ac depletion (p-value = $1x10^{-11}$, **Supplementary Table S16**).

In contrast, HIF1α was not enriched at enhancers showing H3K27ac depletion (**Figure 5E**). Despite sharing many binding sites with HIF2α, HIF1α predominantly localized to promoter-proximal regions whereas HIF2α frequently occupied introns and intergenic regions in 786-O cells (**Figure S8B**), consistent with a promoter-centric occupancy of HIF1α and an enhancer-centric occupancy of HIF2α (**Figure 5F**). Gained enhancers displayed a HIF2α occupancy twice that of tumor-specific promoters (p-value < $1x\ 10^{-16}$, proportions test) in 786-O cells, suggesting that HIF2α may play a greater role at regulating enhancers than promoters.

To extend these HIF1α and HIF2α occupancy patterns findings to a system that expresses endogenous levels of both factors, we then performed HIF1α and HIF2α ChIP-seq in 40911432 ccRCC cells which abundantly co-express both HIFα subunits (**Figure 5B**). Similar to 786-O, in 40911432 cells, HIF1α showed a preferential occupancy at promoter-proximal regions while a large proportion of HIF2α were found in distal regions (introns and distal intergenic regions) (**Figure S8C**). A higher proportion of HIF1α binding sites overlapped with gained promoters than HIF2α (68% of HIF1α vs. 41% of HIF2α, p-value = 0.002, proportions test) (**Figure 5G**). Conversely, a higher proportion of HIF2α binding sites overlapped with gained enhancers than HIF1α (29% of HIF1α vs. 51% of HIF2α, p-value < $2.2\ x\ 10^{-16}$, proportions test). HIF2α's preferential occupancy at enhancers was further substantiated by its higher enrichment at enhancers showing H3K27ac depletion after *VHL* restoration than HIF1α (**Figure 5H**). Specific examples of *VHL*-responsive enhancers bound exclusively by HIF2α but not HIF1α included an enhancer near Ubiquitin Protein Ligase E3 Component N-Recognin 4 (*UBR4*) (**Figure 5I**) and a super-enhancer near C-Maf Inducing Protein (*CMIP*) (**Figure 5J**). Therefore, even in HIF1α/ HIF2α co-expressing ccRCC cells, these results suggest that HIF2α plays a greater role in *VHL*-mediated enhancer remodeling than HIF1α.

HIF2α-HIF1β bound enhancers modulate gene expression

To investigate the extent to which HIF2α silencing is sufficient to recapitulate the effects of *VHL* restoration, we performed H3K27ac ChIP-Seq and RNA-Seq in 786-O cells with *HIF2α* siRNA-mediated knockdown, and analyzed correlations between *HIF2α* siRNA knockdown and *VHL* restoration. When assessed against all genes, there was a low correlation (r = 0.1, *p*-value = 5.2 x 10^{-31}) between *HIF2α* knockdown and *VHL* restoration. Importantly however, this correlation increased to 0.23 (*p*-value = 5.8 x 10^{-14}) for genes nearby HIF2α binding sites (**Figure 6A**). Similar results were obtained at the epigenomic level, where for gained enhancers the correlation was low at 0.06 across all gained enhancers (*p*-value = 1.9 x 10^{-5}) but increased substantially to 0.37 (*p*-value = 9.5 x 10^{-8}) at HIF2α-bound enhancers (**Figure 6B**) and at super-enhancers increased from 0.089 (*p*-value = 0.0025) to 0.25 (*p*-value = 0.00054) at HIF2α-bound super-enhancers (**Figure 6C**). As a visual example, H3K27ac signals at the *ZNF395* super-enhancer were diminished after *VHL* restoration or *HIF2α* knockdown, concomitant with decreased *ZNF395* gene expression (**Figure 6D**). Validation by RT-qPCR showed that *HIF2α* siRNA knockdown downregulated *VEGFA*, *SLC2A1* and *ZNF395* expression to a comparable degree as *VHL* restoration (**Figure 6E**). Decreases in luciferase reporter activity of enhancer elements were also consistent between *HIF2α* siRNA knockdown and *VHL* restoration (**Figure 6F**).

We sought to establish a causal link between HIF2α-bound enhancers and control of gene expression. We performed Clustered Regularly Interspaced Short Palindromic Repeats (CRISPR) mediated genomic depletion of a *ZNF395* enhancer region with the highest HIF2α peak (**Figure 6G**). All four clones with homozygous deleted *ZNF395* enhancer consistently downregulated their *ZNF395* expression compared to clones with the intact enhancer ($p<0.05$), providing evidence that *ZNF395* expression is epigenetically controlled by HIF2α-HIF1β-bound

enhancer (**Figure 6G**). Taken together, these results indicate that that HIF2α is likely an important mediator of *VHL*-driven enhancer remodeling.

VHL restoration reduced P300 recruitment but preserved promoter-enhancer interactions

Finally, we sought to investigate why *VHL* restoration caused a decrease in H3K27ac levels. Previous pull-down assays have reported that both HIF2α and HIF1β can interact with histone acetyltransferase P300 [66-68]. Indeed, P300 frequently marks enhancers [41] and is thought to be recruited by tissue-specific transcription factors [69]. However, chromatin profiles of P300 have not been previously established in kidney cancer cell lines, so the contribution of P300 in shaping enhancers in ccRCC remains unclear. Therefore, we performed P300 ChIP-seq in 786-O cells, and confirmed its enrichment at gained enhancers over lost enhancers (**Figure 7A**). Comparing P300 ChIP-seq with HIF2α CHIP-seq yielded a surprisingly high degree of overlap between HIF2α and P300 (96%), even more than that of HIF2α and HIF1β (89%) (**Figure 7B, 7C**). In contrast, other transcription factors such as c-Jun, ETS1 and NFκB did not exhibit such high degree of overlap (≤60%) (**Figure 7B**).

We compared P300 binding at tumor enhancers with and without *VHL*. Despite increased P300 protein levels in 786-O cells after *VHL* restoration (**Figure 7D**), binding of P300 decreased across all 4 enhancers examined (**Figure 7E**). *HIF2α* depletion by siRNA knockdown also decreased P300 recruitment (**Figure 7F**), suggesting that loss of HIF2α may interfere with P300 recruitment.

We investigated whether *VHL* restoration and the subsequent loss of P300 binding disrupted promoter-enhancer interactions. We performed Capture-C of enhancer regions in paired 786-O cell lines with and without *VHL* restoration. Surprisingly, Capture-C interactions showed a relatively high correlation between *VHL*-deficient and *VHL*-restored 786-O cells at *VHL*-

responsive regions (r = 0.74, Pearson's correlation), even higher than correlations observed at non-*VHL*-responsive regions (r = 0.57, Pearson's correlation) (**Figure 7G**). As a visual example, interactions between the *VEGFA* promoter and enhancer were intact even after *VHL* restoration (**Figure 7H**), indicating that loss of enhancer activity was not sufficient to dissociate promoter-enhancer interactions. Furthermore, many of these promoter-enhancers were lineage-specific, for example the interaction between *SLC2A1* enhancer with its promoter was not detected in KATOIII, a gastric cancer cell line (**Figure S9**). Therefore, promoter-enhancer interactions often pre-exist in kidney cells, frequently in a tissue-specific manner.

Discussion

Understanding epigenomic alterations and their genetic origin can identify new disease mechanisms [32], vulnerabilities [70, 71] and therapeutic strategies [72-74]. Through comprehensive profiling of histone modifications in primary normal-tumor pairs and cell lines, we generated a compendium of ccRCC-associated promoters and enhancers. Our study demonstrates that the most frequent ccRCC mutational event – *VHL* inactivation – leads to genome-wide enhancer and super-enhancer remodeling, which directly imparts ccRCC hallmarks including angiogenesis and metabolic reprogramming. *ZNF395*, epigenetically controlled by a *VHL*-responsive super-enhancer, emerged as a crucial regulator of ccRCC tumorigenesis.

Our work has three main advances. Firstly, to our knowledge, this is the most comprehensive atlas of histone profiles in ccRCC and will likely provide an invaluable resource to the ccRCC field. Using high-resolution multiplexed interactome data (Capture-C [54]) and H3K27ac-expression correlation, we minimized ambiguity in enhancer assignment, and further confirmed the dependency of enhancers on VHL/HIF status by reporter assays. Secondly, using isogenic cell lines, we show that *VHL* loss contributes significantly to enhancer remodeling. Even though

another mutation in ccRCC, *SETD2*, can mediate widespread increases in chromatin accessibility [44] and DNA hypomethylation [75], its relatively low mutation frequency at ~10% in all ccRCC tumors [75] cannot explain epigenetic abnormalities in the vast majority of *SETD2*-widetype tumors. Lastly, an examination of somatically altered super-enhancers enabled us to identify a novel master regulator crucial to the pathogenesis of ccRCC, *ZNF395*. Even though *ZNF395* overexpression in ccRCC has been previously reported [76-78] and its proximity to a super-enhancer was independently noted [40], our study is the first to pinpoint the specific *VHL*-dependent enhancer required for *ZNF395* expression, and to show *ZNF395*'s indispensable functional role for ccRCC tumorigenesis *in vitro* and *in vivo*.

Our data suggests that mechanistically, loss of *VHL* stabilizes HIF2α occupancy at tumor-specific gained enhancers, which in turn recruits histone acetyltransferase P300 [26, 79] to maintain H3K27 acetylation, upregulating expression of ccRCC-specific genes such as *ZNF395* (**Figure 7I**). Restoration of wild-type *VHL* resulted in co-depletion of H3K27ac and H3K4me1 marks and thus abrogation of active enhancer identity at tumor-associated enhancers. Compared to the promoter-centric occupancy of HIF1α, HIF2α is predominantly found at enhancers, pointing towards a key difference between HIF1α and HIF2α. We also found that *HIF2α siRNA* knockdown specifically attenuates the activity of HIF2α-bound enhancers/super-enhancers. Interestingly, the majority of promoter-enhancer interactions remained largely unaltered by *VHL* status, suggesting that these promoter-enhancer couplings are largely stable and pre-formed. This is consistent with a recent report demonstrating that promoter-enhancer interactions remain largely unchanged between normoxia and hypoxia [27]. Our study demonstrating *VHL's* impact on chromatin remodeling also suggests that other cancer genes with high tumor-type specific mutational penetrance, such as *BRAF* in melanoma [80] and *APC* in colon cancer [81] may also act to modify cellular epigenomes to effect broad yet disease-specific cellular changes, despite these genes not being classical chromatin modifiers.

Besides *VHL*, other mutations such as *PBRM1*, *SETD2*, *ARID1A*, *SMARCA4*, *JARID1C*, *KDM6A/UTX* have been reported in ccRCC [45, 82], and these are likely to augment *VHL*'s core transcriptional effects [83], contributing to heterogeneity in disease phenotypes [84] and progression patterns [85]. Using the example of 786-O cells, at least two other mutations in these cells may have a direct impact on chromatin - *MLL3* (p.A3902G) and gain of function *TP53* mutations (p.R248W). *MLL3*, a histone 3 lysine 4 methyltransferase, is directly responsible for formation of the H3K4me1 enhancer mark [86, 87], and plays a critical role for enhancer regulation [88]. Gain of function *TP53* mutants also bind aberrantly to chromatin, especially near methyltransferases *MLL1* and *MLL2,* potentially contributing to tumor growth via chromatin deregulation [89]. Besides mutations, structural variants are also known to alter enhancers via enhancer hijacking [90] or copy number gains [91] in other cancers. Given the multitude of driver and bystander mutations in ccRCC, it is thus unlikely that *VHL* alone can account for all epigenomic changes observed in this tumor type. Nevertheless, by integrating data across multiple ccRCC cell lines, our data suggests that *VHL* inactivation is likely to account for almost a third (32%) of all gained enhancer regions, supporting its role a dominant driver of epigenetic abnormalities in ccRCC despite the presence of other genetic changes.

Our epigenetic maps contain a wellspring of both well-validated and uncharacterized targets that may contribute to ccRCC tumorigenesis. We found extensive enhancer gains around well-characterized hypoxia-related targets [92] (*VEGFA*, *CXCR4* [93], *HK2*), SLC-mediated membrane transporters (*SLC2A1*, *SLC2A2*, *SLC38A1* [94]), *SLC16A* family [95]), and adipogenesis (*PLIN2* [49, 96]). New targets revealed in this study include *SMPDL3A* which could be another important ccRCC-specific oncogene given its role in lipid and cholesterol metabolism [59, 97]. Genes associated with lost super-enhancers, which could only be identified with normal-tumor pairs, implicated potential tumor suppressors (*EHF*, *MAL*, *GCOM1* and *HOXB9*) that warrant further investigation.

One notable finding from this epigenomic study is the tumorigenic requirement of *ZNF395* in ccRCC. *ZNF395* is also known as Huntington's disease gene regulatory region-binding protein-2 (HDBP2) [98] or papillomavirus binding factor (PBF) [99]. *ZNF395* is required for the differentiation of mesenchymal stem cells to adipocytes, by partnering with PPARγ2 to promote adipogenesis [100]. *ZNF395* has been shown to bind to the promoters of Huntington's gene [98], interferon-induced genes, and to cause upregulation of cancer-related genes (*MACC1*, *PEG10*, *CALCOCO1*, *MEF2C*) [101] and pro-angiogenic chemokines including *IL6* and *IL8* under hypoxia [102]. It remains to be elucidated in future studies the precise mechanism contributing to *ZNF395*'s tumorigenic role.

The enhancer landscapes profiled in this study have implications beyond ccRCC. The poorly perfused tumor core makes hypoxia a feature of virtually all solid tumors [103]. MCF7 cells under hypoxia (but not normoxia) share similar H3K27ac profiles as 786-O [27]. While *ZNF395* is highly expressed in ccRCC, its low basal expression can be upregulated upon hypoxia in other cancer types including glioblastoma and skin cancer [101, 102]. Targeting *ZNF395* or its downstream effectors in future studies may be therapeutically relevant to both ccRCC and other hypoxic solid malignancies. Direct targeting of ZNF395 using a peptide-based cancer vaccine is undergoing phase I trials in sarcoma patients [104-106], opening up the possibility of using immunotherapy to target the extracellular fragments of nuclear master regulators. Our study suggests that initiating a similar trial in ccRCC may be worthwhile. Moreover, given the recent progress in targeting transcription factors using various modalities including small molecules and stapled peptides [107-109], inhibitors of *ZNF395* may provide an important therapeutic inroad for ccRCC treatment.

Methods

Cell lines

Commercial cell lines (786-O, A-498, HK-2, PCS-400) were purchased from ATCC. Cell lines were maintained in RPMI (Invitrogen) with 10% FBS with the exception of primary renal proximal tubule epithelial cells, PCS-400, which were maintained in Renal Epithelial Cell Basal Medium (ATCC). Cell line authentication was performed by short tandem repeat (STR) analysis (Cancer Science Institute of Singapore) in 2015 against publicly available STR profiles. Mycoplasma testing was performed using the MycoSensor PCR assay kit (Stratagene).

Establishment of tumor-derived cell lines from primary tumors

Tumor cells were disassociated from primary tumors by collagenase, seeded and maintained in RPMI with 10% FBS. At 80-90% confluency, the cells were passaged at a 1:3 ratio. Cultured cells were considered to be successfully immortalized after 60 passages. Correct pairing of tumor tissues and cell lines was achieved by comparing the percentage identity of single nucleotide polymorphisms (SNPs) based on targeted sequencing. All tumor-cell line pairs showed identities of > 90% whereas shuffling of pairing showed identities < 80%. Tumors and cell lines from 12364284 and 40911432 showed the same *VHL* mutations but 86049102 tissue (named 86049102T) is *VHL* mutant while the cognate 86049102 cell line (named 86049102L) is *VHL* wild-type.

Stable *VHL* restoration in ccRCC lines

786-O cells (WT2, *VHL*+) and 786-O cells (RC3, *VHL*−) were kindly provided by Dr. Michael Ohh (University of Toronto). Stable transduction of *VHL* was performed in A-498, 12364284 and 40911432 cells as follows: HA-*VHL* wt-pBabe-puro plasmid (a gift from Dr. William Kaelin, Dana Farber Cancer Institute, Addgene plasmid # 19234) was transfected into PlatA cells (RV-102, Cell Biolabs) at 2 µg DNA/well of a 6-well plate using Lipofectamine 3000 (LifeTechnologies). A medium change was performed 10-16 hrs after transfection. The supernatant from PlatA cells containing retroviruses was harvested 48 hours later, and added to ccRCC cells, which were then selected with puromycin for 3 days post transduction.

Histone Nano-ChIP-Seq

Nano-ChIP-Seq was performed as previously described [110] with slight modifications. Fresh-frozen cancer and normal tissues were dissected using a razor blade to obtain ~5 mg of tissue. The tissues were fixed in 1% formaldehyde for 10 min at room temperature. Fixation was

stopped by addition of glycine to a final concentration of 125 nM. Tissue pieces were washed 3 times with TBSE buffer. Pulverized tissues were lysed in 100 µl lysis buffer and sonicated for 16 cycles (30s on, 30s off) using a Bioruptor (Diagenode). The following antibodies were used: H3K27ac (ab4729, Abcam), H3K4me3 (07-473, Millipore), H3K4me1 (ab8895, Abcam) and H3K27me3 (07-449, Millipore). The total volume of immunoprecipitation was 1 ml and the amount of antibody used was 2 µg. The input DNA was precleared with protein G Dynabeads (Life Technologies) for 1 hr at 4°C and then incubated with antibodies conjugated protein G beads overnight at 4°C. The beads were washed 3 times with cold wash buffer. After recovery of ChIP and input DNA, whole-genome-amplification was performed using the WGA4 kit (Sigma-Aldrich) and BpmI-WGA primters. Amplified DNA was digested with BpmI (New England Biolabs (NEB)). After that, 30 ng of the amplified DNA was used with the NEBNext ChIP-Seq library prep reagent set (NEB). ChIP-seq in cell lines were performed using the same Nano-ChIP-seq protocol described above but with $1x10^6$ cells. Each library was sequenced to an average depth of 20-30 million raw reads on HiSeq2500 using 101bp single end reads.

Histone ChIP-Seq analysis

Sequencing tags were mapped against the human reference genome (hg19) using Burrows-Wheeler Aligner (BWA-mem) [111](version 0.7.10). Reads were trimmed 10 bp from the front and the back to produce 81 bp. Only reads with mapQ >10 and with duplicates removed by rmdup were used for subsequent analysis. Significant peaks were called using CCAT (p-value < 0.05) [112]. The strength and quality of immunoprecipitation was assessed using CHANCE [113].

Transcription factor Chip-Seq

For each transcription factor, $3x10^7$ cells were cross-linked with 1% formaldehyde for 10 min at room temperature, and stopped by adding glycine to a final concentration of 125 nM. Chromatin was extracted and sonicated to ~500bp (Vibra cell, SONICS). The following antibodies were used for chromatin immunoprecipitation, c-Jun (sc-1694, Santa Cruz), NFκB p65 (sc-372, Santa Cruz), ETS1 (sc-350, Santa Cruz), HIF1α (610959, BD Biosciences), and HIF2α (NB100-122, Novus Bio) and P300 (sc-585, Santa Cruz). The total volume of immunoprecipitation was 1.5 ml and the amount of antibody used was 15 µg. Input DNAs were precleared with protein G Dynabeads (LifeTechnologies) for 2 hr at 4°C and then incubated with antibody-conjugated protein G beads overnight at 4°C. The beads were washed 6 times with wash buffer at room temperature. At least 10 ng of the DNA was used with the NEBNext ChIP-Seq library prep

reagent set (NEB). Each library was sequenced to an average depth of 30-50 million reads on a HiSeq2500 using 101bp single end reads.

Capture C

Capture-C was performed as previously described [54]. Briefly, $1x10^7$ cells were crosslinked by 2% formaldehyde, followed by lysis, homogenization, DpnII digestion, ligation, and de-crosslinking. DNA was sonicated using a Covaris to 150-200bp to produce DNA suitable for oligo capture. A total of 3 µg of sheared DNA was used for sequencing library preparation (New England Biolabs). Enhancer sequences were double captured by hybridisation to customized biotinylated oligos (IDT) and enriched with Dynabeads (Life Technologies). Captured DNA was sequenced to an average depth of 2 million reads per probe on the Hiseq Illumina platform using 150 bp paired-end reads.

Capture C analysis and Gene assignment

Preprocessing of raw reads was performed to remove adaptor sequences (trim_galore, http://www.bioinformatics.babraham.ac.uk/projects/trim_galore/) and overlapping reads were merged using FLASH [114]. In order to achieve short read mapping to the hg19 reference genome, the resulting preprocessed reads were then *in-silico* digested with DpnII and aligned using Bowtie (using p1, m2, best and strata settings). Aligned reads were processed using Capture-C analyser [115] to (i) remove PCR duplicates, (ii) classify sub fragments as 'capture' if they were contained within the capture fragment; 'proximity exclusion' if they were within 1Kb on either side of the capture fragment; or 'reporter' if they were outside of the 'capture' and 'proximity exclusion' regions, and (iii) normalize read counts per 100,000 interactions in bigwig format. We additionally used the r3Cseq package [116] on the capture and reporter fragments to identify significant interactions of the viewpoint against a scaled background (q-value <0.05). Gene assignment is defined by the overlap of significant Capture C peaks with genes with start and end defined by GENCODE v19. Interactions were plotted using Epigenome Gateway v40.0.

Identification of differentially enriched regions

Significant H3K27ac peaks called by CCAT were merged across all normal-tumor samples. The same was performed with H3K4me1 and H3K4me3 ChIP-seq data. Transcription start sites were based on GENCODE v19. Promoters were defined as regions of overlap between H3K27ac and H3K4me3 and also overlapping with ±2.0 Kb around the transcription start site. Enhancers were defined as regions of overlap between H3K27ac and H3K4me1 but not

overlapping with promoters. To minimize stromal contamination, we performed further filtering using cell line data, where enhancers and promoters not overlapping with H3K27ac peaks in any of the cell lines were discarded. Wiggle files of window size 50 bp were generated using MEDIPs [117] from bam files. The input-subtracted signal for each promoter or enhancer region was computed using bigWigAverageOverBed to yield reads per kilobase per million (RPKM). The RPKM of H3K27ac, H3K4me1 and H3K4me3 ChIP-Seq from promoters and enhancers were corrected for batch effects using Combat. Tumor specific regions were defined as regions that have a fold difference of ≥2, and a difference of 0.5 RPKM from patient-matched normal tissue. Normal regions were defined as regions that have a fold difference of ≤0.5, and a difference of -0.5 RPKM from the corresponding regions in patient-matched tumor. Recurrently gained regions were defined as gain in ≥ 5/10 patients and no loss in any patients. Recurrently lost regions were defined as loss in ≥ 5/10 patients and no gain in any patients. Statistical testing for each *cis*-regulatory region was performed using paired *t*-tests with Benjamini-Hochberg correction. The differential regions were visualized using NGSplot [118].

Identification of super-enhancer regions

Super-enhancer regions were identified using ROSE [33] (with promoter excluded), using H3K27ac peak regions merged from all patients (both normal and tumor tissue). Wiggle files of window size 50 bp were generated using MEDIPs [117] from bam files. The input-subtracted signal for each super-enhancer was computed using bigWigAverageOverBed (sum of reads over covered bases). The super-enhancer regions were ranked by the average difference of normal-tumor H3K27ac ChIP-seq signals. Gained super-enhancers were defined as regions that have average differential H3K27ac ChIP-seq signals >0. Lost super-enhancers were defined as regions that have average differential H3K27ac ChIP-seq signals <0.

Additional methods can be found in Supplementary Methods.

Date Accession

ChIP-seq and RNAseq data are available at Gene Expression Omnibus (GSE86095).

Reviewer access:

http://www.ncbi.nlm.nih.gov/geo/query/acc.cgi?token=mrcpieayxjmnpmt&acc=GSE86095

Acknowledgements

We thank Hui Hoon Chua and Angie Tan for their administrative support. We thank the Sequencing and Scientific Computing teams at the Genome Institute of Singapore for sequencing services and data management capabilities, and the Duke-NUS Genome Biology Facility for sequencing services. We thank the Advanced Molecular Pathology Laboratory of IMCB for pathology evaluation. P.T., B.T.T., X.Y. and J.T. conceived the experiments. J.K., Z.L., X.Y., J.T., D.H., M.X., G.W., Y.N.L., J.H.H., A.P.L., M.S.W.N., S.S.M., C.Z.H., G.L., and B.C.T. performed the experiments. K.L., W.F.O., P.G., J.S.L, T.N., A.Q. and S.R. performed or supervised the bioinformatics analysis. Y.S.C, J.Z.Q and S.T.T. performed next generation sequencing. J.O.J.D. and J.R.H. advised on Capture-C experiments. K.T.E.C and P.H.T. supervised pathology assessment and provided pathology evaluation. C.W.S.C provided the clinical specimens. C.X., J.Y.G, Q.Y., S.L, I.B.H.T., D.L.S., A. L. and G. S. provided important technical advice and reagents. X.Y. and P.T. wrote the manuscript.

References

1. Ferlay J, S.I., Ervik M, Dikshit R, Eser S, Mathers C, Rebelo M, Parkin DM, Forman D, Bray, F. GLOBOCAN, *Cancer Incidence and Mortality Worldwide: IARC CancerBase No. 11.* 2014.
2. Society, A.C., *Survival rates for kidney cancer by stage.*
3. Rini, B.I. and K. Flaherty, *Clinical effect and future considerations for molecularly-targeted therapy in renal cell carcinoma.* Urol Oncol, 2008. **26**(5): p. 543-9.
4. Rini, B.I. and M.B. Atkins, *Resistance to targeted therapy in renal-cell carcinoma.* Lancet Oncol, 2009. **10**(10): p. 992-1000.
5. Gerlinger, M., et al., *Genomic architecture and evolution of clear cell renal cell carcinomas defined by multiregion sequencing.* Nat Genet, 2014. **46**(3): p. 225-33.
6. Gerlinger, M., et al., *Intratumor heterogeneity and branched evolution revealed by multiregion sequencing.* N Engl J Med, 2012. **366**(10): p. 883-92.
7. Gu, Y.F., et al., *Modeling Renal Cell Carcinoma in Mice: Bap1 and Pbrm1 Inactivation Drive Tumor Grade.* Cancer Discov, 2017.
8. Nargund, A.M., et al., *The SWI/SNF Protein PBRM1 Restrains VHL-Loss-Driven Clear Cell Renal Cell Carcinoma.* Cell Rep, 2017. **18**(12): p. 2893-2906.
9. Harlander, S., et al., *Combined mutation in Vhl, Trp53 and Rb1 causes clear cell renal cell carcinoma in mice.* Nat Med, 2017.
10. Iwai, K., et al., *Identification of the von Hippel-lindau tumor-suppressor protein as part of an active E3 ubiquitin ligase complex.* Proc Natl Acad Sci U S A, 1999. **96**(22): p. 12436-41.
11. Lisztwan, J., et al., *The von Hippel-Lindau tumor suppressor protein is a component of an E3 ubiquitin-protein ligase activity.* Genes Dev, 1999. **13**(14): p. 1822-33.
12. Maxwell, P.H., et al., *The tumour suppressor protein VHL targets hypoxia-inducible factors for oxygen-dependent proteolysis.* Nature, 1999. **399**(6733): p. 271-5.
13. Jaakkola, P., et al., *Targeting of HIF-alpha to the von Hippel-Lindau ubiquitylation complex by O2-regulated prolyl hydroxylation.* Science, 2001. **292**(5516): p. 468-72.
14. Ebert, B.L. and H.F. Bunn, *Regulation of transcription by hypoxia requires a multiprotein complex that includes hypoxia-inducible factor 1, an adjacent transcription factor, and p300/CREB binding protein.* Mol Cell Biol, 1998. **18**(7): p. 4089-96.
15. Ema, M., et al., *Molecular mechanisms of transcription activation by HLF and HIF1alpha in response to hypoxia: their stabilization and redox signal-induced interaction with CBP/p300.* EMBO J, 1999. **18**(7): p. 1905-14.
16. Biswas, S., et al., *Effects of HIF-1alpha and HIF2alpha on Growth and Metabolism of Clear-Cell Renal Cell Carcinoma 786-0 Xenografts.* J Oncol, 2010. **2010**: p. 757908.
17. Metallo, C.M., et al., *Reductive glutamine metabolism by IDH1 mediates lipogenesis under hypoxia.* Nature, 2012. **481**(7381): p. 380-4.
18. Rankin, E.B., et al., *Hypoxia-inducible factor 2 regulates hepatic lipid metabolism.* Mol Cell Biol, 2009. **29**(16): p. 4527-38.
19. Schodel, J., et al., *Common genetic variants at the 11q13.3 renal cancer susceptibility locus influence binding of HIF to an enhancer of cyclin D1 expression.* Nat Genet, 2012. **44**(4): p. 420-5, S1-2.
20. Roe, J.S., et al., *p53 stabilization and transactivation by a von Hippel-Lindau protein.* Mol Cell, 2006. **22**(3): p. 395-405.
21. Tamiya, H., et al., *Analysis of the Runx2 promoter in osseous and non-osseous cells and identification of HIF2A as a potent transcription activator.* Gene, 2008. **416**(1-2): p. 53-60.

22. Ko, C.Y., et al., *Integration of CNS survival and differentiation by HIF2alpha.* Cell Death Differ, 2011. **18**(11): p. 1757-70.
23. Imtiyaz, H.Z., et al., *Hypoxia-inducible factor 2alpha regulates macrophage function in mouse models of acute and tumor inflammation.* J Clin Invest, 2010. **120**(8): p. 2699-714.
24. Xie, L. and J.F. Collins, *Transcription factors Sp1 and Hif2alpha mediate induction of the copper-transporting ATPase (Atp7a) gene in intestinal epithelial cells during hypoxia.* J Biol Chem, 2013. **288**(33): p. 23943-52.
25. Ruas, J.L., et al., *Complex regulation of the transactivation function of hypoxia-inducible factor-1 alpha by direct interaction with two distinct domains of the CREB-binding protein/p300.* J Biol Chem, 2010. **285**(4): p. 2601-9.
26. Freedman, S.J., et al., *Structural basis for recruitment of CBP/p300 by hypoxia-inducible factor-1 alpha.* Proc Natl Acad Sci U S A, 2002. **99**(8): p. 5367-72.
27. Platt, J.L., et al., *Capture-C reveals preformed chromatin interactions between HIF-binding sites and distant promoters.* EMBO Rep, 2016. **17**(10): p. 1410-1421.
28. Salama, R., et al., *Heterogeneous Effects of Direct Hypoxia Pathway Activation in Kidney Cancer.* PLoS One, 2015. **10**(8): p. e0134645.
29. Grampp, S., et al., *Genetic variation at the 8q24.21 renal cancer susceptibility locus affects HIF binding to a MYC enhancer.* Nat Commun, 2016. **7**: p. 13183.
30. Heinz, S., et al., *The selection and function of cell type-specific enhancers.* Nat Rev Mol Cell Biol, 2015. **16**(3): p. 144-54.
31. Heintzman, N.D., et al., *Histone modifications at human enhancers reflect global cell-type-specific gene expression.* Nature, 2009. **459**(7243): p. 108-12.
32. Lin, C.Y., et al., *Active medulloblastoma enhancers reveal subgroup-specific cellular origins.* Nature, 2016. **530**(7588): p. 57-62.
33. Whyte, W.A., et al., *Master transcription factors and mediator establish super-enhancers at key cell identity genes.* Cell, 2013. **153**(2): p. 307-19.
34. Liu, F., et al., *EGFR Mutation Promotes Glioblastoma through Epigenome and Transcription Factor Network Remodeling.* Mol Cell, 2015. **60**(2): p. 307-18.
35. Riggi, N., et al., *EWS-FLI1 utilizes divergent chromatin remodeling mechanisms to directly activate or repress enhancer elements in Ewing sarcoma.* Cancer Cell, 2014. **26**(5): p. 668-81.
36. Niu, X., et al., *The von Hippel-Lindau tumor suppressor protein regulates gene expression and tumor growth through histone demethylase JARID1C.* Oncogene, 2012. **31**(6): p. 776-86.
37. Ramakrishnan, S., et al., *HDAC 1 and 6 modulate cell invasion and migration in clear cell renal cell carcinoma.* BMC Cancer, 2016. **16**: p. 617.
38. Beyer, S., et al., *The histone demethylases JMJD1A and JMJD2B are transcriptional targets of hypoxia-inducible factor HIF.* J Biol Chem, 2008. **283**(52): p. 36542-52.
39. Luo, W., et al., *Histone demethylase JMJD2C is a coactivator for hypoxia-inducible factor 1 that is required for breast cancer progression.* Proc Natl Acad Sci U S A, 2012. **109**(49): p. E3367-76.
40. Rhie, S.K., et al., *Identification of activated enhancers and linked transcription factors in breast, prostate, and kidney tumors by tracing enhancer networks using epigenetic traits.* Epigenetics Chromatin, 2016. **9**: p. 50.
41. Heintzman, N.D., et al., *Distinct and predictive chromatin signatures of transcriptional promoters and enhancers in the human genome.* Nat Genet, 2007. **39**(3): p. 311-8.
42. Creyghton, M.P., et al., *Histone H3K27ac separates active from poised enhancers and predicts developmental state.* Proc Natl Acad Sci U S A, 2010. **107**(50): p. 21931-6.
43. Akhtar-Zaidi, B., et al., *Epigenomic enhancer profiling defines a signature of colon cancer.* Science, 2012. **336**(6082): p. 736-9.

44. Simon, J.M., et al., *Variation in chromatin accessibility in human kidney cancer links H3K36 methyltransferase loss with widespread RNA processing defects.* Genome Res, 2014. **24**(2): p. 241-50.
45. Cancer Genome Atlas Research, N., *Comprehensive molecular characterization of clear cell renal cell carcinoma.* Nature, 2013. **499**(7456): p. 43-9.
46. Iyer, M.K., et al., *The landscape of long noncoding RNAs in the human transcriptome.* Nat Genet, 2015. **47**(3): p. 199-208.
47. Purdue, M.P., et al., *Genome-wide association study of renal cell carcinoma identifies two susceptibility loci on 2p21 and 11q13.3.* Nat Genet, 2011. **43**(1): p. 60-5.
48. McLean, C.Y., et al., *GREAT improves functional interpretation of cis-regulatory regions.* Nat Biotechnol, 2010. **28**(5): p. 495-501.
49. Qiu, B., et al., *HIF2alpha-Dependent Lipid Storage Promotes Endoplasmic Reticulum Homeostasis in Clear-Cell Renal Cell Carcinoma.* Cancer Discov, 2015. **5**(6): p. 652-67.
50. Kim, J.W., et al., *HIF-1-mediated expression of pyruvate dehydrogenase kinase: a metabolic switch required for cellular adaptation to hypoxia.* Cell Metab, 2006. **3**(3): p. 177-85.
51. Papandreou, I., et al., *HIF-1 mediates adaptation to hypoxia by actively downregulating mitochondrial oxygen consumption.* Cell Metab, 2006. **3**(3): p. 187-97.
52. Wise, D.R., et al., *Myc regulates a transcriptional program that stimulates mitochondrial glutaminolysis and leads to glutamine addiction.* Proc Natl Acad Sci U S A, 2008. **105**(48): p. 18782-7.
53. Gameiro, P.A., et al., *In vivo HIF-mediated reductive carboxylation is regulated by citrate levels and sensitizes VHL-deficient cells to glutamine deprivation.* Cell Metab, 2013. **17**(3): p. 372-85.
54. Davies, J.O., et al., *Multiplexed analysis of chromosome conformation at vastly improved sensitivity.* Nat Methods, 2016. **13**(1): p. 74-80.
55. Parker, S.C., et al., *Chromatin stretch enhancer states drive cell-specific gene regulation and harbor human disease risk variants.* Proc Natl Acad Sci U S A, 2013. **110**(44): p. 17921-6.
56. Albino, D., et al., *ESE3/EHF controls epithelial cell differentiation and its loss leads to prostate tumors with mesenchymal and stem-like features.* Cancer Res, 2012. **72**(11): p. 2889-900.
57. Cangemi, R., et al., *Reduced expression and tumor suppressor function of the ETS transcription factor ESE-3 in prostate cancer.* Oncogene, 2008. **27**(20): p. 2877-85.
58. Dalgin, G.S., et al., *Identification and characterization of renal cell carcinoma gene markers.* Cancer Inform, 2007. **3**: p. 65-92.
59. Noto, P.B., et al., *Regulation of sphingomyelin phosphodiesterase acid-like 3A gene (SMPDL3A) by liver X receptors.* Mol Pharmacol, 2012. **82**(4): p. 719-27.
60. Iliopoulos, O., et al., *Tumour suppression by the human von Hippel-Lindau gene product.* Nat Med, 1995. **1**(8): p. 822-6.
61. Gnarra, J.R., et al., *Post-transcriptional regulation of vascular endothelial growth factor mRNA by the product of the VHL tumor suppressor gene.* Proc Natl Acad Sci U S A, 1996. **93**(20): p. 10589-94.
62. Schoenfeld, A., E.J. Davidowitz, and R.D. Burk, *A second major native von Hippel-Lindau gene product, initiated from an internal translation start site, functions as a tumor suppressor.* Proc Natl Acad Sci U S A, 1998. **95**(15): p. 8817-22.
63. Heinz, S., et al., *Simple combinations of lineage-determining transcription factors prime cis-regulatory elements required for macrophage and B cell identities.* Mol Cell, 2010. **38**(4): p. 576-89.
64. An, J., et al., *Hyperactivated JNK is a therapeutic target in pVHL-deficient renal cell carcinoma.* Cancer Res, 2013. **73**(4): p. 1374-85.

65. Elvert, G., et al., *Cooperative interaction of hypoxia-inducible factor-2alpha (HIF-2alpha) and Ets-1 in the transcriptional activation of vascular endothelial growth factor receptor-2 (Flk-1).* J Biol Chem, 2003. **278**(9): p. 7520-30.
66. Steunou, A.L., et al., *Identification of the hypoxia-inducible factor 2alpha nuclear interactome in melanoma cells reveals master proteins involved in melanoma development.* Mol Cell Proteomics, 2013. **12**(3): p. 736-48.
67. Kung, A.L., et al., *Small molecule blockade of transcriptional coactivation of the hypoxia-inducible factor pathway.* Cancer Cell, 2004. **6**(1): p. 33-43.
68. Tohkin, M., et al., *Aryl hydrocarbon receptor is required for p300-mediated induction of DNA synthesis by adenovirus E1A.* Mol Pharmacol, 2000. **58**(4): p. 845-51.
69. Visel, A., et al., *ChIP-seq accurately predicts tissue-specific activity of enhancers.* Nature, 2009. **457**(7231): p. 854-8.
70. Bitler, B.G., et al., *Synthetic lethality by targeting EZH2 methyltransferase activity in ARID1A-mutated cancers.* Nat Med, 2015. **21**(3): p. 231-8.
71. Bernt, K.M., et al., *MLL-rearranged leukemia is dependent on aberrant H3K79 methylation by DOT1L.* Cancer Cell, 2011. **20**(1): p. 66-78.
72. Loven, J., et al., *Selective inhibition of tumor oncogenes by disruption of super-enhancers.* Cell, 2013. **153**(2): p. 320-34.
73. McCabe, M.T., et al., *EZH2 inhibition as a therapeutic strategy for lymphoma with EZH2-activating mutations.* Nature, 2012. **492**(7427): p. 108-12.
74. Daigle, S.R., et al., *Selective killing of mixed lineage leukemia cells by a potent small-molecule DOT1L inhibitor.* Cancer Cell, 2011. **20**(1): p. 53-65.
75. *Comprehensive molecular characterization of clear cell renal cell carcinoma.* Nature, 2013. **499**(7456): p. 43-9.
76. Kim, Y., et al., *Loss of CDC14B expression in clear cell renal cell carcinoma: meta-analysis of microarray data sets.* Am J Clin Pathol, 2014. **141**(4): p. 551-8.
77. Skubitz, K.M., et al., *Differential gene expression identifies subgroups of renal cell carcinoma.* J Lab Clin Med, 2006. **147**(5): p. 250-67.
78. Wozniak, M.B., et al., *Integrative genome-wide gene expression profiling of clear cell renal cell carcinoma in Czech Republic and in the United States.* PLoS One, 2013. **8**(3): p. e57886.
79. Gu, J., J. Milligan, and L.E. Huang, *Molecular mechanism of hypoxia-inducible factor 1alpha -p300 interaction. A leucine-rich interface regulated by a single cysteine.* J Biol Chem, 2001. **276**(5): p. 3550-4.
80. Hodis, E., et al., *A landscape of driver mutations in melanoma.* Cell, 2012. **150**(2): p. 251-63.
81. *Comprehensive molecular characterization of human colon and rectal cancer.* Nature, 2012. **487**(7407): p. 330-7.
82. Varela, I., et al., *Exome sequencing identifies frequent mutation of the SWI/SNF complex gene PBRM1 in renal carcinoma.* Nature, 2011. **469**(7331): p. 539-42.
83. Gao, W., et al., *Inactivation of the PBRM1 tumor suppressor gene amplifies the HIF-response in VHL-/- clear cell renal carcinoma.* Proc Natl Acad Sci U S A, 2017.
84. Bi, M., et al., *Genomic characterization of sarcomatoid transformation in clear cell renal cell carcinoma.* Proc Natl Acad Sci U S A, 2016. **113**(8): p. 2170-5.
85. Ho, T.H., et al., *High-resolution profiling of histone h3 lysine 36 trimethylation in metastatic renal cell carcinoma.* Oncogene, 2016. **35**(12): p. 1565-74.
86. Herz, H.M., et al., *Enhancer-associated H3K4 monomethylation by Trithorax-related, the Drosophila homolog of mammalian Mll3/Mll4.* Genes Dev, 2012. **26**(23): p. 2604-20.
87. Hu, D., et al., *The MLL3/MLL4 branches of the COMPASS family function as major histone H3K4 monomethylases at enhancers.* Mol Cell Biol, 2013. **33**(23): p. 4745-54.

88. Dorighi, K.M., et al., *Mll3 and Mll4 Facilitate Enhancer RNA Synthesis and Transcription from Promoters Independently of H3K4 Monomethylation.* Mol Cell, 2017. **66**(4): p. 568-576 e4.
89. Zhu, J., et al., *Gain-of-function p53 mutants co-opt chromatin pathways to drive cancer growth.* Nature, 2015. **525**(7568): p. 206-11.
90. Northcott, P.A., et al., *Enhancer hijacking activates GFI1 family oncogenes in medulloblastoma.* Nature, 2014. **511**(7510): p. 428-34.
91. Zhang, X., et al., *Identification of focally amplified lineage-specific super-enhancers in human epithelial cancers.* Nat Genet, 2016. **48**(2): p. 176-82.
92. Schodel, J., et al., *Hypoxia, Hypoxia-inducible Transcription Factors, and Renal Cancer.* Eur Urol, 2015.
93. Vanharanta, S., et al., *Epigenetic expansion of VHL-HIF signal output drives multiorgan metastasis in renal cancer.* Nat Med, 2013. **19**(1): p. 50-6.
94. Broer, A., F. Rahimi, and S. Broer, *Deletion of Amino Acid Transporter ASCT2 (SLC1A5) Reveals an Essential Role for Transporters SNAT1 (SLC38A1) and SNAT2 (SLC38A2) to Sustain Glutaminolysis in Cancer Cells.* J Biol Chem, 2016. **291**(25): p. 13194-205.
95. Adijanto, J. and N.J. Philp, *The SLC16A family of monocarboxylate transporters (MCTs)--physiology and function in cellular metabolism, pH homeostasis, and fluid transport.* Curr Top Membr, 2012. **70**: p. 275-311.
96. Morrissey, J.J., et al., *Evaluation of Urine Aquaporin-1 and Perilipin-2 Concentrations as Biomarkers to Screen for Renal Cell Carcinoma: A Prospective Cohort Study.* JAMA Oncol, 2015. **1**(2): p. 204-12.
97. Traini, M., et al., *Sphingomyelin phosphodiesterase acid-like 3A (SMPDL3A) is a novel nucleotide phosphodiesterase regulated by cholesterol in human macrophages.* J Biol Chem, 2014. **289**(47): p. 32895-913.
98. Tanaka, K., et al., *Novel nuclear shuttle proteins, HDBP1 and HDBP2, bind to neuronal cell-specific cis-regulatory element in the promoter for the human Huntington's disease gene.* J Biol Chem, 2004. **279**(8): p. 7275-86.
99. Sichtig, N., N. Korfer, and G. Steger, *Papillomavirus binding factor binds to SAP30 and represses transcription via recruitment of the HDAC1 co-repressor complex.* Arch Biochem Biophys, 2007. **467**(1): p. 67-75.
100. Hasegawa, R., et al., *Identification of ZNF395 as a novel modulator of adipogenesis.* Exp Cell Res, 2013. **319**(3): p. 68-76.
101. Jordanovski, D., et al., *The hypoxia-inducible transcription factor ZNF395 is controlled by IkB kinase-signaling and activates genes involved in the innate immune response and cancer.* PLoS One, 2013. **8**(9): p. e74911.
102. Herwartz, C., et al., *The Transcription Factor ZNF395 Is Required for the Maximal Hypoxic Induction of Proinflammatory Cytokines in U87-MG Cells.* Mediators Inflamm, 2015. **2015**: p. 804264.
103. Vaupel, P., et al., *Current status of knowledge and critical issues in tumor oxygenation. Results from 25 years research in tumor pathophysiology.* Adv Exp Med Biol, 1998. **454**: p. 591-602.
104. Tsukahara, T., et al., *HLA-A*0201-restricted CTL epitope of a novel osteosarcoma antigen, papillomavirus binding factor.* J Transl Med, 2009. **7**: p. 44.
105. Tsukahara, T., et al., *Identification of human autologous cytotoxic T-lymphocyte-defined osteosarcoma gene that encodes a transcriptional regulator, papillomavirus binding factor.* Cancer Res, 2004. **64**(15): p. 5442-8.
106. Tsukahara, T., et al., *Specific targeting of a naturally presented osteosarcoma antigen, papillomavirus binding factor peptide, using an artificial monoclonal antibody.* J Biol Chem, 2014. **289**(32): p. 22035-47.

107. Chen, W., et al., *Targeting renal cell carcinoma with a HIF-2 antagonist.* Nature, 2016. **539**(7627): p. 112-117.
108. Cho, H., et al., *On-target efficacy of a HIF-2alpha antagonist in preclinical kidney cancer models.* Nature, 2016. **539**(7627): p. 107-111.
109. Bernal, F., et al., *A stapled p53 helix overcomes HDMX-mediated suppression of p53.* Cancer Cell, 2010. **18**(5): p. 411-22.
110. Ng, J.H., et al., *In vivo epigenomic profiling of germ cells reveals germ cell molecular signatures.* Dev Cell, 2013. **24**(3): p. 324-33.
111. Li, H., *Aligning sequence reads, clone sequences and assembly contigs with BWA-MEM.* q-bio.GN, 2013.
112. Xu, H., et al., *A signal-noise model for significance analysis of ChIP-seq with negative control.* Bioinformatics, 2010. **26**(9): p. 1199-204.
113. Diaz, A., A. Nellore, and J.S. Song, *CHANCE: comprehensive software for quality control and validation of ChIP-seq data.* Genome Biol, 2012. **13**(10): p. R98.
114. Magoc, T. and S.L. Salzberg, *FLASH: fast length adjustment of short reads to improve genome assemblies.* Bioinformatics, 2011. **27**(21): p. 2957-63.
115. Hughes, J.R., et al., *Analysis of hundreds of cis-regulatory landscapes at high resolution in a single, high-throughput experiment.* Nat Genet, 2014. **46**(2): p. 205-12.
116. Thongjuea, S., et al., *r3Cseq: an R/Bioconductor package for the discovery of long-range genomic interactions from chromosome conformation capture and next-generation sequencing data.* Nucleic Acids Res, 2013. **41**(13): p. e132.
117. Lienhard, M., et al., *MEDIPS: genome-wide differential coverage analysis of sequencing data derived from DNA enrichment experiments.* Bioinformatics, 2014. **30**(2): p. 284-6.
118. Shen, L., et al., *ngs.plot: Quick mining and visualization of next-generation sequencing data by integrating genomic databases.* BMC Genomics, 2014. **15**: p. 284.

Figure legends

Figure 1: *VHL* deficient ccRCC tumors exhibit an aberrant cis-regulatory landscape

(A) Putative active promoters are defined by co-occurrence of H3K4me3, H3K27ac and proximity to transcription start sites (TSSs) within 2 kb. Putative active enhancers are defined by the presence of H3K4me1, H3K27ac and exclusivity with promoters. **(B)** PCA analysis using all 17,497 promoters and 66,448 enhancers classify normal and tumors into distinct clusters. Patient IDs: (1-12364284; 2-17621953; 3-20431713; 4-40911432; 5-57398667; 6-70528835; 7-74575859; 8-77972083; 9-86049102; 10-75416923) **(C)** Heat maps show H3K27ac levels of altered promoters and enhancers in a paired patient tissue (patient 40911432, yellow high, black low). **(D)** The H3K27ac levels, chromatin accessibility (FAIRE-seq), DNA methylation of gained promoters and enhancers, and gene expression of the nearest ccRCC lncRNA are compared between normal and tumor tissues. ****p*-value < 0.001, two-sided *t*-test. **(E)** Shown are tracks of histone ChIP-seq (H3K27ac, H3K4me1, H3K4me3) and RNA-Seq at the *CCND1* locus in a tumor-normal pair of patient 40911432. The histone ChIP-seq profiles of normal adult kidney tissue from the Epigenome Roadmap are displayed above the normal tissue generated by Nano-ChIP-seq for comparison. A cell line was derived from the tumor tissue and its histone profile is displayed below its matching primary tissue. This enhancer is known to interact with the *CCND1* promoter from a previous study (Schodel, 2012 [19]), and is situated close to a RCC susceptibility SNP rs7105934 [47].

Figure 2: Enhancer aberration is a signature of ccRCC

(A) Enriched pathways associated with gained promoters and enhancers revealed by GREAT (ranked by binomial FDR *q*-value). Red bars refer to ccRCC-specific pathways. **(B)** *De novo* enhancers are acquired in a ccRCC tumor tissue upstream of *VEGFA*. Capture-C confirmed interactions of this *VEGFA* enhancer (E) with its promoter (P) in 786-O cells. The arcs represent significant interactions detected by r3Cseq (q<0.05). The input-subtracted H3K27ac signals of this enhancer are highly correlated with *VEGFA* gene expression (Spearman's correlation). **(C)** Similar to **(B)**, a *de novo* tumor enhancer interacts with the *SLC2A1/GLUT1* promoter.

Figure 3: Tumor super-enhancers identify key oncogenic drivers

(A) A total of 1,451 super-enhancers are identified by ROSE and ranked by their differential H3K27ac intensity between normal and tumor tissues. Genes associated with the top gained and lost super-enhancers are listed. **(B)** TCGA RNA-seq data indicates that genes associated with top 10 gained enhancers are upregulated in tumors while genes associated with top 10 lost enhancers are downregulated. This tumor-specificity is restricted to ccRCC, but not the other two RCC subtypes, papillary and chromophobe. **(C)** Expression of *ZNF395* and *SMPDL3A* are measured in a panel of normal kidney cell lines (black) and ccRCC cell lines (red) by RT-qPCR. **(D)** Pooled siRNA against *ZNF395* inhibits colony formation of A-498 and 786-O but not HK-2 normal immortalized kidney cells. Pooled siRNA against *SMPLD3A* inhibits colony formation of A-498 but not 786-O. **(E)** H3K27ac ChIP-seq shows an active *ZNF395* super-enhancer only in ccRCC cells (A-498 and 786-O) but not normal kidney cells (PCS-400, HK-2). **(F)** TCGA RNA-seq data shows exclusive overexpression of *ZNF395* amongst 12 cancer types. **(G-I)** *ZNF395* inhibition by two shRNA clones decreases colony formation **(G)**, *in vitro* proliferation **(H)** and increases apoptosis measured by cleavage of Caspase3/7 substrate **(I)**. **p*-value < 0.05, two-sided *t*-test. (**J**) *ZNF395* inhibition by shRNA leads to total elimination of A-498 tumors *in vivo* and delayed 786-O tumor growth. NC: n=7, shZNF395-1: n=7, shZNF395-2: n=6

Figure 4: *VHL* deficiency remodels ccRCC enhancers

(A) Log fold changes of H3K27ac ChIP-seq signals at gained promoters, enhancers and super-enhancers as defined in the primary ccRCC dataset after *VHL* restoration in 786-O cells. Red dots represent *cis*-

regulatory elements with significant changes (*p*-value <0.05, negative binomial) in H3K27ac levels after *VHL* restoration. The number and percentage of altered regions (*p*-value <0.05, negative binomial) are shown at the upper and lower right corners. **(B)** Read coverage of H3K27ac ChIP-seq at *VHL*-responsive enhancers in *VHL*-mutant ccRCC cell lines (red) compared to *VHL*-wild-type ccRCC (grey), and normal kidney cell lines (green) and 31 other cancer cell lines (black). **(C)** Changes in expression of genes linked to *VHL*-responsive tumor enhancers after *VHL* restoration in 786-O cells. **p*-value < 0.05, two-sided *t*-test. **(D-G)** Examples of lost *VHL*-responsive enhancer/super-enhancers are associated with *EGFR* **(D)**, *CCND1* **(E)**, *ITGB3* **(F)** and *VEGFA* **(G)** in 786-O cells. **(H)** Log fold changes of H3K27ac (red), H3K4me1 (blue) and H3K27me3 (brown) signals at gained enhancers showing H3K27ac depletion after *VHL* restoration in 786-O cells.

Figure 5: HIF2α is enriched at enhancers of *VHL*-responsive tumor tumors

(A) Motif analysis of gained enhancers using HOMER reveals significant enrichment of AP-1 family, ETS family, NFκB and HIF1α/2α (hypergeometric test). Lost enhancers were used as background in the motif search to identify tumor-specific transcription factors. **(B)** Protein expressions of putative transcription factors enriched at gained enhancers in 9 tumor cell lines (4 commercial cell lines and 5 patient-derived cell lines*) and 2 normal cell lines. ACHN is a papillary RCC cell line. **(C)** ChIP-seq validated the enrichment of transcription factors in gained enhancers over lost enhancers. **(D)** Protein expression of transcription factors are shown in 786-O and 12364284 cells with and without wild-type *VHL*. **(E)** Transcription factor binding at *VHL*-responsive gained enhancers shows enrichment of HIF2α and HIF1β at enhancers with H3K27ac depletion (red) over regions with H3K27ac enrichment (black) after *VHL* restoration. **(F)** ChIP-Seq data shows distribution of exogenous HIF1α and endogenous HIF2α binding at altered promoters and enhancers in 786-O cells that have been genetically engineered to overexpress HIF1α. **(G)** ChIP-Seq shows distribution of endogenous HIF1α and HIF2α binding at altered promoters and enhancers in 40911432 cells. **(H)** Transcription factor binding at *VHL*-responsive enhancers shows higher enrichment of HIF2α than HIF1α at enhancers with H3K27ac depletion after *VHL* restoration (red) over regions with H3K27ac enrichment after *VHL* restoration (black) **(I)** Example of a *VHL*-responsive enhancer near *UBR4* with only HIF2α binding but not HIF1α binding **(J)** Example of a *VHL*-responsive super-enhancer near *CMIP* with only HIF2α binding but not HIF1α binding.

Figure 6: HIF2α-HIF1β bound enhancers modulate gene expression

(A) Pearson's correlation of gene expression changes after either *VHL* restoration or *HIF2α* siRNA knockdown at all genes or genes adjacent to HIF2α binding sites. **(B)** Pearson's correlation of H3K27ac changes after *VHL* restoration and *HIF2α* siRNA knockdown at either all gained enhancers or HIF2α-bound enhancers adjacent to binding sites. **(C)** Pearson's correlation of H3K27ac changes after *VHL* restoration and *HIF2α* siRNA knockdown at either all gained super-enhancers or HIF2α-bound super-enhancers adjacent to binding sites. **(D)** Changes in RNAseq and H3K27ac ChIP-Seq signals after *VHL* restoration or *HIF2α* siRNA knockdown at *ZNF395* super-enhancer (SE), together with binding profiles of transcription factors enriched at enhancers. **(E)** Both *VHL* restoration and *HIF2α* siRNA knockdown decreases expression of genes with HIF2α-bound enhancers in 786-O cells. *p-value < 0.05, two-sided *t*-test. **(F)** Both *VHL* restoration and *HIF2α* siRNA knockdown decrease enhancer activities measured by luciferase reporter assay in 786-O cells. **p*-value < 0.05, two-sided *t*-test. **(G)** RT-qPCR measurement of *ZNF395* expression in 4 wild-type clones (black) and 4 clones with *ZNF395* enhancer depleted by CRISPR (red). Depleted region has the highest HIF2α binding at *ZNF395* super-enhancer in 786-O cells (deleted region indicated in **D**). **p*-value < 0.05, two-sided *t*-test.

Figure 7: *VHL* restoration reduces P300 recruitment but preserves promoter-enhancer interactions

(A) Enrichment of P300 binding at gained and lost enhancers based on ChIP-Seq. **(B)** Percentage of overlap between HIF2α and other transcription factors. **(C)** ChIP-Seq binding profiles of HIF2α and P300.

(D) Protein expression of P300 with and without *VHL* in 786-O and 12364284 cells measured by immunoblotting. **(E)** ChIP-qPCR of P300 binding at enhancers with and without *VHL* restoration in 786-O cells. NC – negative control regions. **(F)** ChIP-qPCR of P300 binding at enhancers with and without *HIF2α* siRNA knockdown in 786-O cells. NC – negative control regions. **(G)** Correlation of enhancer interactions measured by Capture-C (RPM – reads per million) between 786-O cells with and without *VHL* restoration at both *VHL*-responsive and non-*VHL*-responsive enhancers **(H)** Capture-C shows that *VEGFA* enhancer-promoter interactions are maintained even after *VHL* restoration. E – enhancer; P – promoter. **(I)** Schematics of *VHL*-driven enhancer aberration in ccRCC.

Figure 1

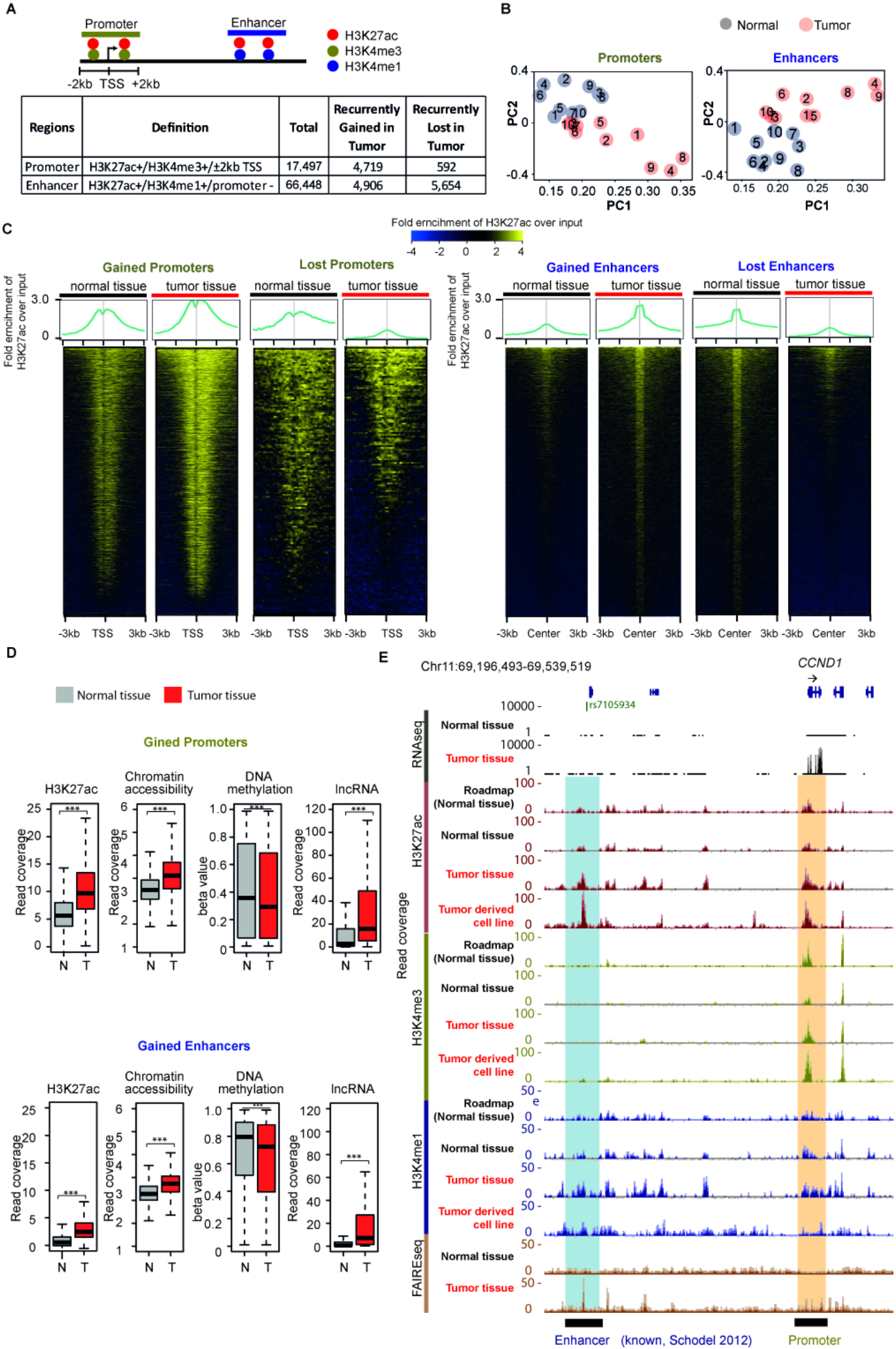

Regions	Definition	Total	Recurrently Gained in Tumor	Recurrently Lost in Tumor
Promoter	H3K27ac+/H3K4me3+/±2kb TSS	17,497	4,719	592
Enhancer	H3K27ac+/H3K4me1+/promoter -	66,448	4,906	5,654

Figure 2

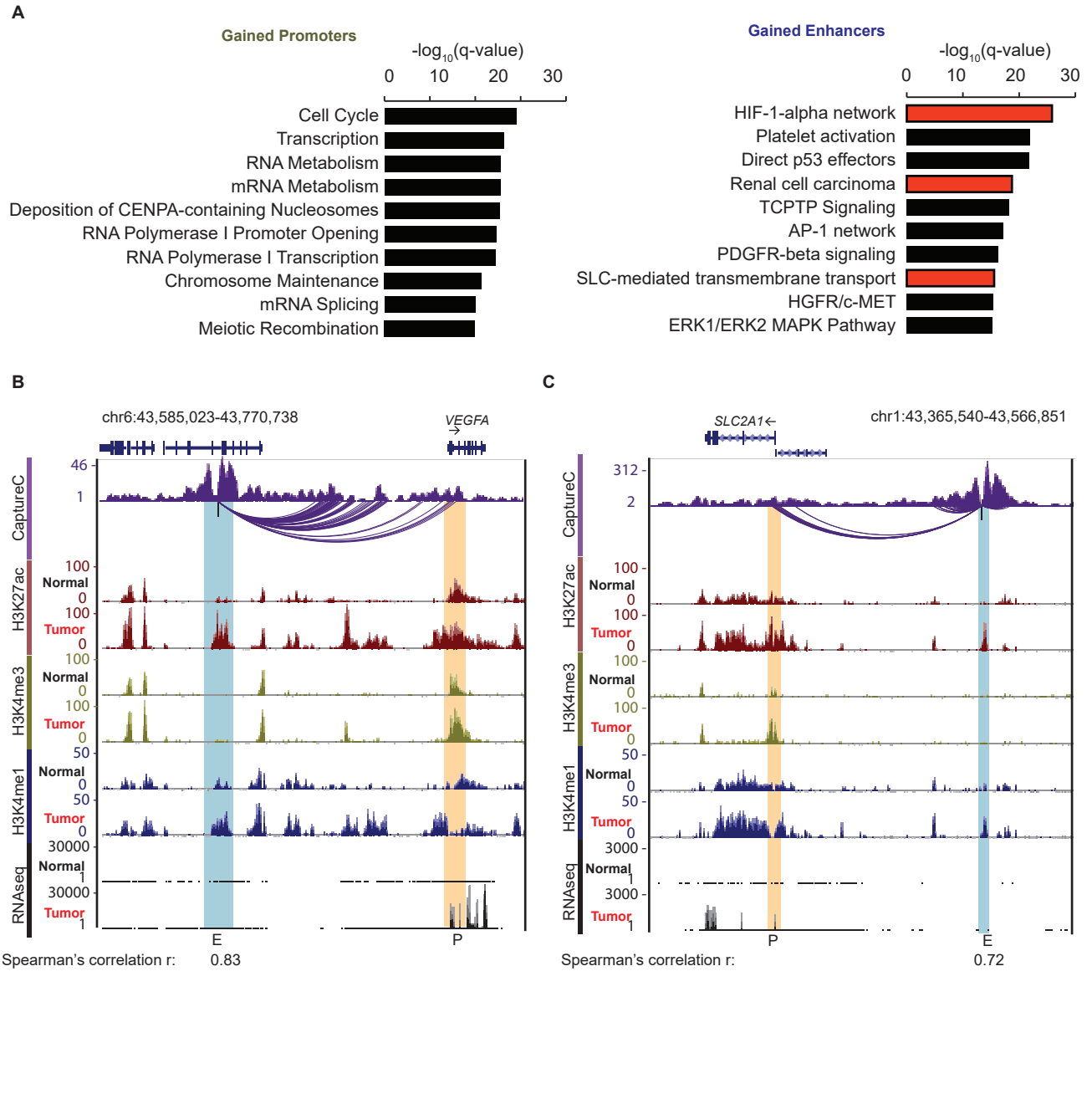
A
Gained Promoters
-log10(q-value)
0
10
20
30
Cell Cycle
Transcription
RNA Metabolism
mRNA Metabolism
Deposition of CENPA-containing Nucleosomes
RNA Polymerase I Promoter Opening
RNA Polymerase I Transcription
Chromosome Maintenance
mRNA Splicing
Meiotic Recombination
Gained Enhancers
-log10(q-value)
0
10
20
30
HIF-1-alpha network
Platelet activation
Direct p53 effectors
Renal cell carcinoma
TCPTP Signaling
AP-1 network
PDGFR-beta signaling
SLC-mediated transmembrane transport
HGFR/c-MET
ERK1/ERK2 MAPK Pathway
B
chr6:43,585,023-43,770,738
VEGFA
CaptureC
H3K27ac
H3K4me3
H3K4me1
RNAseq
Normal
Tumor
E
P
Spearman's correlation r:
0.83
C
chr1:43,365,540-43,566,851
SLC2A1
CaptureC
H3K27ac
H3K4me3
H3K4me1
RNAseq
Normal
Tumor
P
E
Spearman's correlation r:
0.72

Figure 3

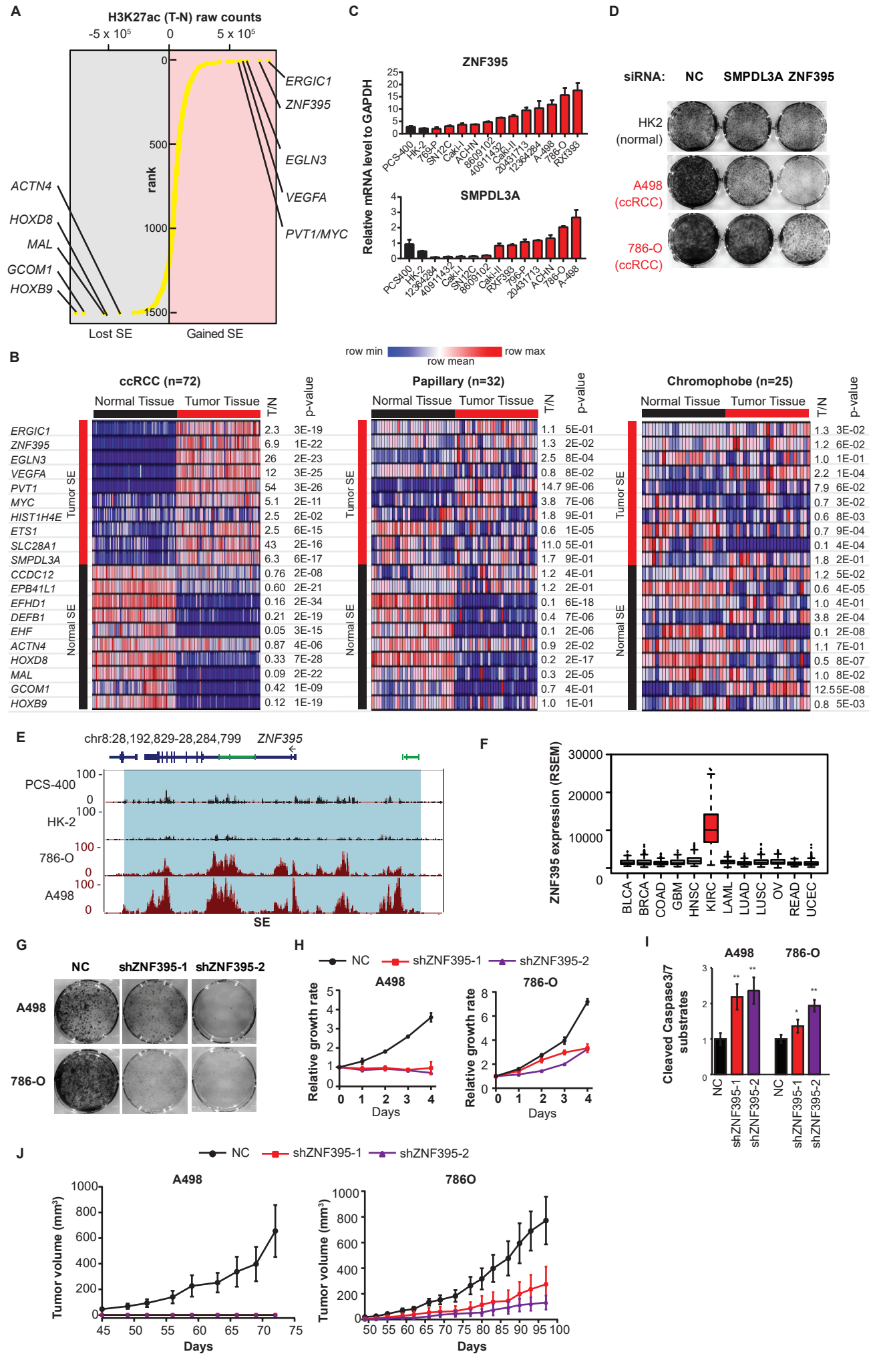
A
H3K27ac (T-N) raw counts
-5 x 10^5
0
5 x 10^5
rank
ERGIC1
ZNF395
EGLN3
VEGFA
PVT1/MYC
ACTN4
HOXD8
MAL
GCOM1
HOXB9
Lost SE
Gained SE
C
ZNF395
SMPDL3A
Relative mRNA level to GAPDH
PCS-400
HK-2
769-P
SN12C
Caki-I
ACHN
Caki-II
A-498
786-O
RXF393
D
siRNA:
NC
SMPDL3A
ZNF395
HK2 (normal)
A498 (ccRCC)
786-O (ccRCC)
B
row min
row mean
row max
ccRCC (n=72)
Papillary (n=32)
Chromophobe (n=25)
Normal Tissue
Tumor Tissue
T/N
p-value
Tumor SE
Normal SE
ERGIC1 2.3 3E-19 1.1 5E-01 1.3 3E-02
ZNF395 6.9 1E-22 1.3 2E-02 1.2 6E-02
EGLN3 26 2E-23 2.5 8E-04 1.0 1E-01
VEGFA 12 3E-25 0.8 8E-02 2.2 1E-04
PVT1 54 3E-26 14.7 9E-06 7.9 6E-02
MYC 5.1 2E-11 3.8 7E-06 0.7 3E-02
HIST1H4E 2.5 2E-02 1.8 9E-01 0.6 8E-03
ETS1 2.5 6E-15 0.6 1E-05 0.7 9E-04
SLC28A1 43 2E-16 11.0 5E-01 0.1 4E-04
SMPDL3A 6.3 6E-17 1.7 9E-01 1.8 2E-01
CCDC12 0.76 2E-08 1.2 4E-01 1.2 5E-02
EPB41L1 0.60 2E-21 1.2 2E-01 0.6 4E-05
EFHD1 0.16 2E-34 0.1 6E-18 1.0 4E-01
DEFB1 0.21 2E-19 0.4 7E-06 3.8 2E-04
EHF 0.05 3E-15 0.1 2E-06 0.1 2E-08
ACTN4 0.87 4E-06 0.9 2E-02 1.1 7E-01
HOXD8 0.33 7E-28 0.2 2E-17 0.5 8E-07
MAL 0.09 2E-22 0.3 2E-05 1.0 8E-02
GCOM1 0.42 1E-09 0.7 4E-01 12.5 5E-08
HOXB9 0.12 1E-19 1.0 1E-01 0.8 5E-03
E
chr8:28,192,829-28,284,799
ZNF395
PCS-400
HK-2
786-O
A498
SE
F
ZNF395 expression (RSEM)
BLCA
BRCA
COAD
GBM
HNSC
KIRC
LAML
LUAD
LUSC
OV
READ
UCEC
G
NC
shZNF395-1
shZNF395-2
A498
786-O
H
NC
shZNF395-1
shZNF395-2
A498
786-O
Relative growth rate
Days
I
A498
786-O
Cleaved Caspase3/7 substrates
J
NC
shZNF395-1
shZNF395-2
A498
786O
Tumor volume (mm3)
Days

Figure 4

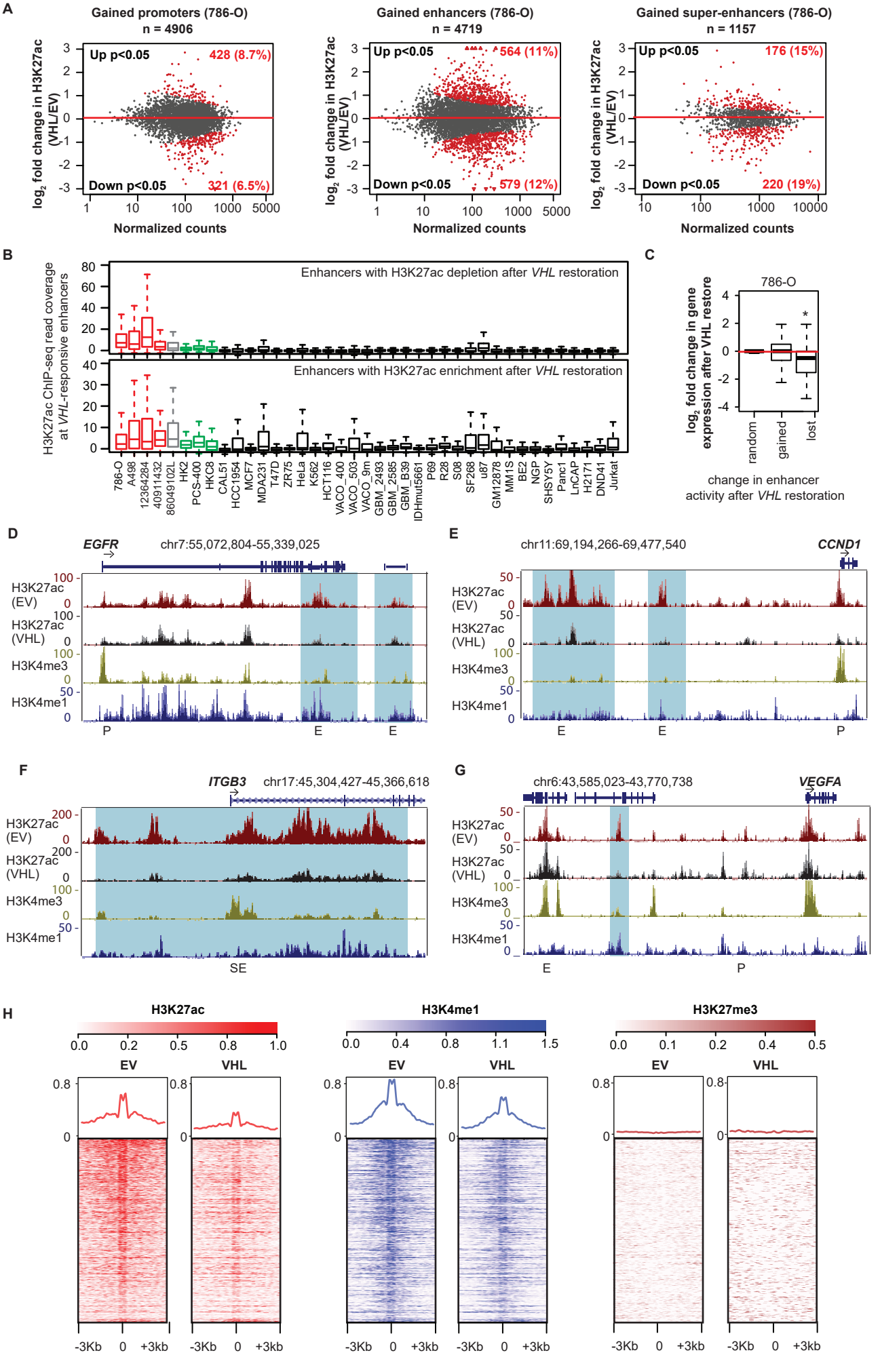
A
Gained promoters (786-O)
n = 4906
Up p<0.05
428 (8.7%)
Down p<0.05
321 (6.5%)
log2 fold change in H3K27ac (VHL/EV)
Normalized counts
Gained enhancers (786-O)
n = 4719
Up p<0.05
564 (11%)
Down p<0.05
579 (12%)
Gained super-enhancers (786-O)
n = 1157
Up p<0.05
176 (15%)
Down p<0.05
220 (19%)
B
H3K27ac ChIP-seq read coverage at VHL-responsive enhancers
Enhancers with H3K27ac depletion after VHL restoration
Enhancers with H3K27ac enrichment after VHL restoration
786-O
A498
12364284
40911432
86049102L
HK2
PCS-400
HKC8
CAL51
HCC1954
MCF7
MDA231
T47D
ZR75
HeLa
K562
HCT116
VACO_400
VACO_503
VACO_9m
GBM_2493
GBM_2585
GBM_B39
IDHmut5661
P69
R28
S08
SF268
u87
GM12878
MM1S
BE2
NGP
SHSY5Y
Panc1
LnCAP
H2171
DND41
Jurkat
C
786-O
log2 fold change in gene expression after VHL restore
random
gained
lost
change in enhancer activity after VHL restoration
D
EGFR
chr7:55,072,804-55,339,025
H3K27ac (EV)
H3K27ac (VHL)
H3K4me3
H3K4me1
P
E
E
E
chr11:69,194,266-69,477,540
CCND1
E
E
P
F
ITGB3
chr17:45,304,427-45,366,618
SE
G
chr6:43,585,023-43,770,738
VEGFA
E
P
H
H3K27ac
H3K4me1
H3K27me3
EV
VHL
-3Kb
0
+3kb

Figure 5

A

Motif	Family	Members	p-value
	bZIP	Fosl2, Jun-AP1, Bach2, Fra1, BATF, Atf3, AP-1, MafK	1E-63
	ETS	Ets1-distal, PU.1, Fli1	1E-32
	RHD	NFkB-p65-Rel	1E-25
	bHLH	HIF2α, HIF1α	1E-23
	IRF	ISRE	1E-21

B

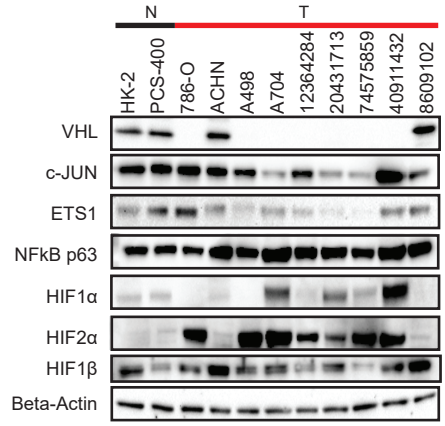

C

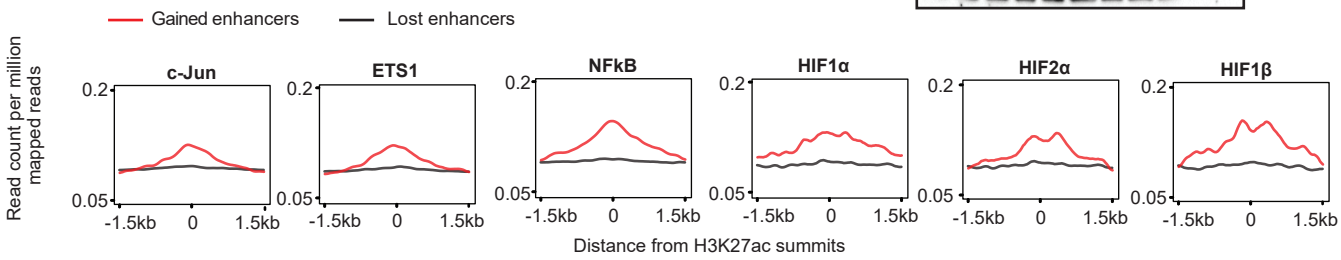

D

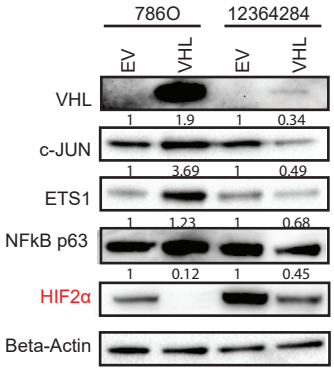

E

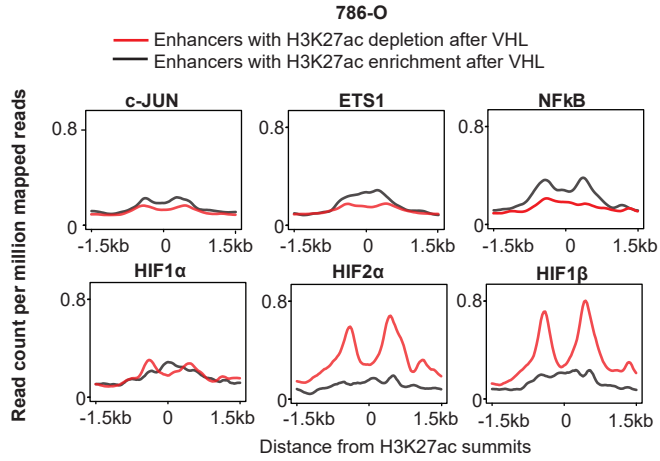

F

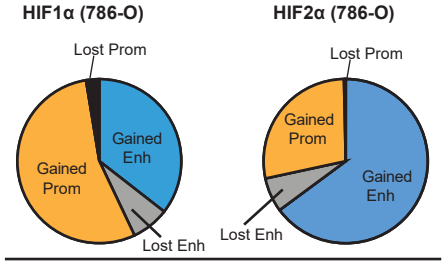

G

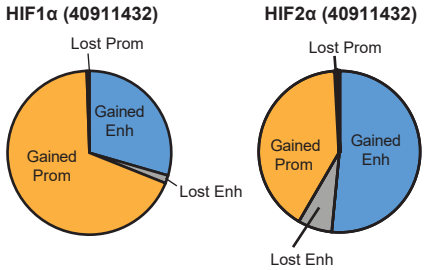

H

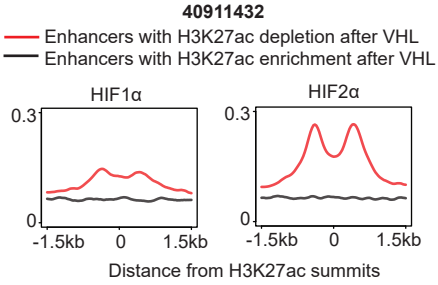

I

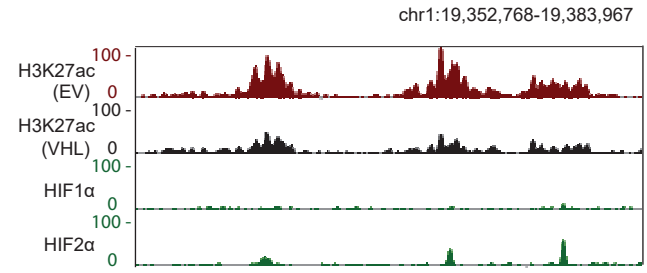

J

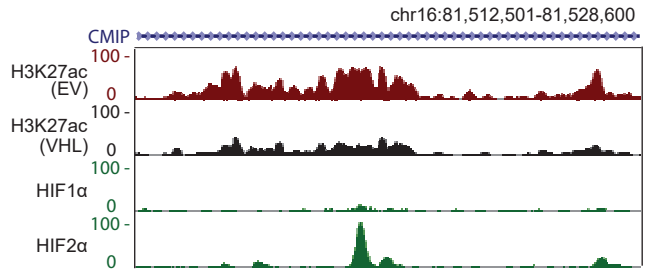

Figure 6

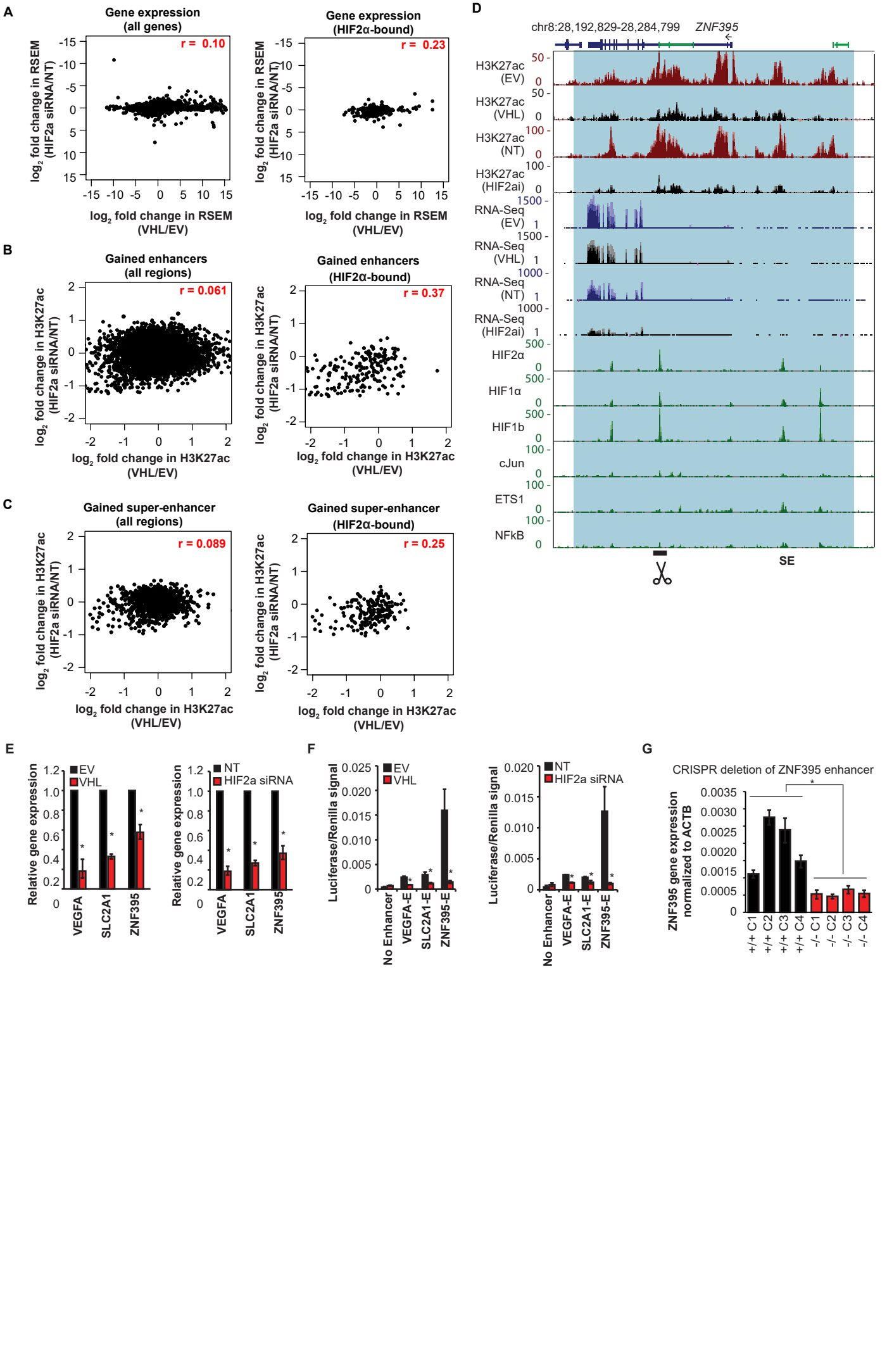
A
Gene expression (all genes)
r = 0.10
Gene expression (HIF2α-bound)
r = 0.23
log2 fold change in RSEM (HIF2a siRNA/NT)
log2 fold change in RSEM (VHL/EV)
B
Gained enhancers (all regions)
r = 0.061
Gained enhancers (HIF2α-bound)
r = 0.37
log2 fold change in H3K27ac (HIF2a siRNA/NT)
log2 fold change in H3K27ac (VHL/EV)
C
Gained super-enhancer (all regions)
r = 0.089
Gained super-enhancer (HIF2α-bound)
r = 0.25
D
chr8:28,192,829-28,284,799
ZNF395
H3K27ac (EV)
H3K27ac (VHL)
H3K27ac (NT)
H3K27ac (HIF2ai)
RNA-Seq (EV)
RNA-Seq (VHL)
RNA-Seq (NT)
RNA-Seq (HIF2ai)
HIF2α
HIF1α
HIF1b
cJun
ETS1
NFkB
SE
E
Relative gene expression
EV
VHL
NT
HIF2a siRNA
VEGFA
SLC2A1
ZNF395
F
Luciferase/Renilla signal
No Enhancer
VEGFA-E
SLC2A1-E
ZNF395-E
G
CRISPR deletion of ZNF395 enhancer
ZNF395 gene expression normalized to ACTB
+/+ C1
+/+ C2
+/+ C3
+/+ C4
-/- C1
-/- C2
-/- C3
-/- C4

Figure 7

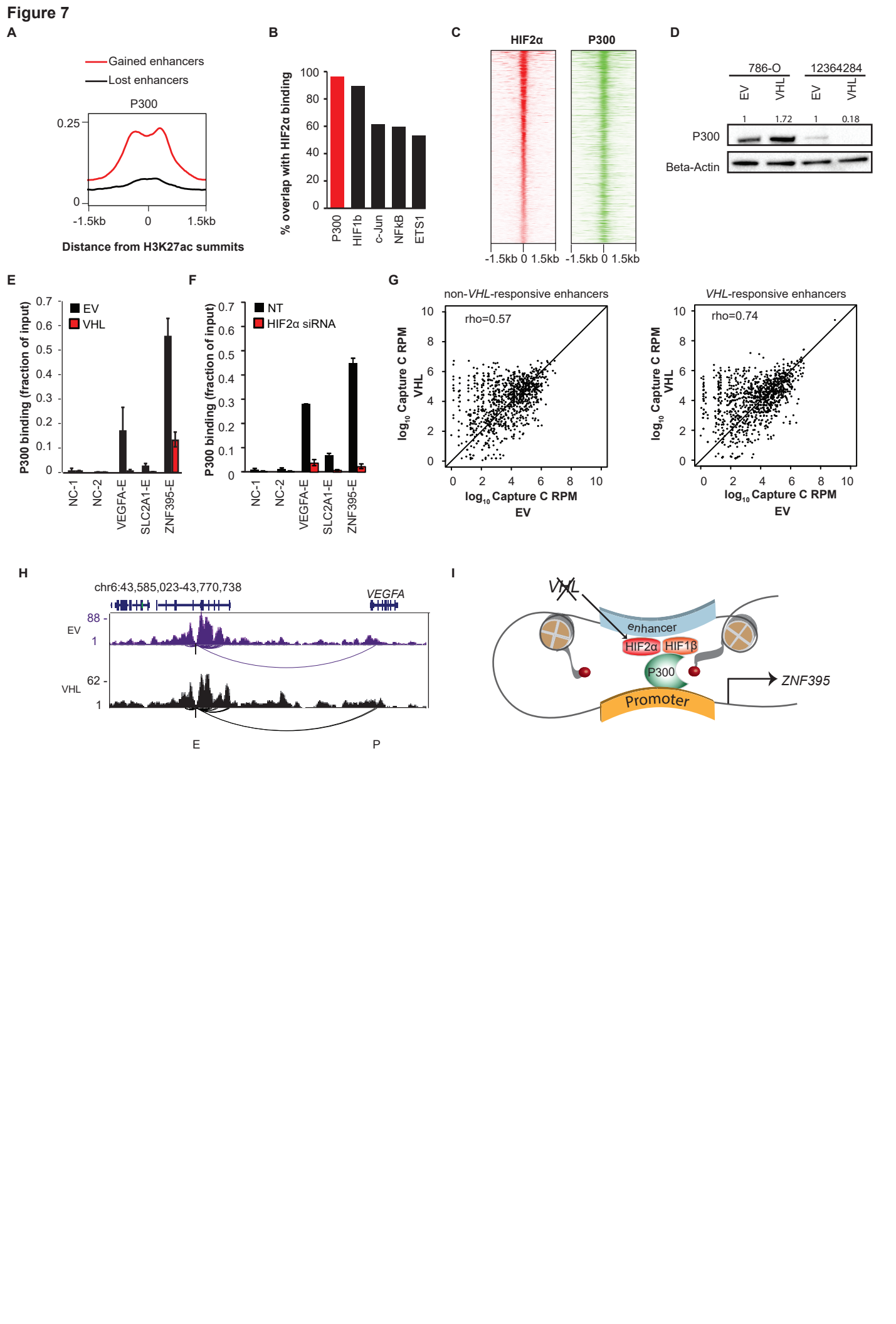
A
Gained enhancers
Lost enhancers
P300
0.25
0
-1.5kb
0
1.5kb
Distance from H3K27ac summits
B
% overlap with HIF2α binding
100
80
60
40
20
0
P300
HIF1b
c-Jun
NFkB
ETS1
C
HIF2α
P300
-1.5kb 0 1.5kb
-1.5kb 0 1.5kb
D
786-O
12364284
EV
VHL
EV
VHL
1
1.72
1
0.18
P300
Beta-Actin
E
EV
VHL
P300 binding (fraction of input)
0.7
0.6
0.5
0.4
0.3
0.2
0.1
0
NC-1
NC-2
VEGFA-E
SLC2A1-E
ZNF395-E
F
NT
HIF2α siRNA
P300 binding (fraction of input)
NC-1
NC-2
VEGFA-E
SLC2A1-E
ZNF395-E
G
non-VHL-responsive enhancers
rho=0.57
log10 Capture C RPM VHL
log10 Capture C RPM EV
VHL-responsive enhancers
rho=0.74
log10 Capture C RPM VHL
log10 Capture C RPM EV
H
chr6:43,585,023-43,770,738
VEGFA
EV
88
1
VHL
62
1
E
P
I
VHL
enhancer
HIF2α
HIF1β
P300
Promoter
ZNF395